

Paleomagnetism indicates no Neogene vertical axis rotations of the northeastern Tibetan Plateau

Guillaume Dupont-Nivet¹ and Robert F. Butler

Department of Geosciences, University of Arizona, Tucson, Arizona, USA

An Yin

Department of Earth and Space Sciences, University of California, Los Angeles, California, USA

Xuanhua Chen

Institute of Geomechanics, Beijing, China

Received 13 January 2003; revised 28 February 2003; accepted 2 April 2003; published 20 August 2003.

[1] Paleomagnetic data were obtained from 108 paleomagnetic sites collected in Cretaceous to Tertiary red beds from seven localities distributed in three general regions adjacent to the Altyn Tagh fault at the northern edge of the Tibetan Plateau. In the Hexi corridor, 12 sites in Oligocene strata at Yaoquanzi (39.97°N; 97.68°E) yield a mean paleomagnetic direction ($I = 33.0^\circ$; $D = 8.6^\circ$, $\alpha_{95} = 6.0^\circ$) with concordant declination, and 36 sites in Early Cretaceous mudstones of the Longshou Shan (39.09°N; 100.50°E) provide a concordant paleomagnetic direction ($I = 53.4^\circ$; $D = 6.8^\circ$, $\alpha_{95} = 3.8^\circ$). Across the Nan Shan fold-thrust belt, Miocene paleomagnetic directions from 39 sites distributed among four localities have a concordant mean declination ($I = 40.6^\circ$; $D = 7.2^\circ$, $\alpha_{95} = 5.8^\circ$). In the Altyn Tagh range, 21 sites in Oligocene strata at Xorkoli (38.93°N; 91.43°E) yield a paleomagnetic direction with concordant declination ($I = 49.7^\circ$; $D = 5.0^\circ$, $\alpha_{95} = 5.4^\circ$). These results combined with existing regional paleomagnetic data indicate that (1) the Hexi corridor along with the North China block has not undergone tectonic vertical axis rotation since at least Early Cretaceous time and is separated from the Xining-Lanzhou basin and eastern Tibet by an important post-Early Cretaceous tectonic boundary; (2) the Nan Shan fold-thrust belt and the Qaidam Basin have not experienced wholesale vertical axis rotation during Neogene time; and (3) absence of vertical axis rotations in areas adjacent to the Altyn Tagh fault indicates that sinistral shear strain between the Tarim Basin and the northern Tibetan Plateau is concentrated on the fault. These results are consistent with Asian tectonic models that combine distributed lithospheric deformation and thickening with narrow and weak shear zones. *INDEX*

TERMS: 1525 Geomagnetism and Paleomagnetism: Paleomagnetism applied to tectonics (regional, global); 8102 Tectonophysics: Continental contractional orogenic belts; 8110 Tectonophysics: Continental tectonics—general (0905); *KEYWORDS:* tectonics, Asia, paleomagnetism, Tibetan Plateau, Cenozoic

Citation: Dupont-Nivet, G., R. F. Butler, A. Yin, and X. Chen, Paleomagnetism indicates no Neogene vertical axis rotations of the northeastern Tibetan Plateau, *J. Geophys. Res.*, 108(B8), 2386, doi:10.1029/2003JB002399, 2003.

1. Introduction

[2] The 2500 km northward penetration of India into Asia since ~65–55 Ma resulted in the largest collisional orogenic system in the world, the Himalayan-Tibetan orogen [Argand, 1924; Molnar and Tapponnier, 1975; Besse and Courtillot, 1988; Le Pichon et al., 1992; Yin and Harrison, 2000]. Because knowledge of the evolution of this orogen is linked to understanding of the physical properties of continental

lithosphere in continent-continent collisions, major efforts have been made to retrace the formation of the different components of the orogen [England and Houseman, 1985; Molnar et al., 1993; Royden et al., 1997; Tapponnier et al., 2001]. Of particular interest is the long-standing question of whether the penetration of India is accommodated through lithospheric deformation and thickening distributed over a viscous continuum or through localized deformation on major lithospheric faults with high slip rates bounding quasi-rigid blocks [England and Houseman, 1988; Peltzer and Tapponnier, 1988]. These tectonic models make contrasting predictions about the kinematic evolution of the orogen that can be tested.

[3] The recent velocity field and strain distribution of the orogen are described mainly through Global Positioning

¹Now at Utrecht University, Faculty of Earth Sciences, Paleomagnetic Laboratory - "Fort Hoofdijk", Utrecht, Netherlands.

System (GPS) measurements over the past decade [Bendick et al., 2000; Chen et al., 2000; Shen et al., 2001], seismic moment tensor analyses of earthquakes during last few decades [Molnar and Deng, 1984; Molnar and Lyon-Caen, 1989; Holt and Haines, 1993; Holt et al., 1995], and neotectonic studies of Quaternary slip rates on major faults [Molnar et al., 1987; Peltzer et al., 1989; van der Woerd et al., 1998; Meriaux et al., 2000]. Despite these major efforts, no consensus has been reached. Observed deformation rates can be fit by numerical models assuming either distributed or localized deformation [Avouac and Tapponnier, 1993; Kong and Bird, 1996; Peltzer and Saucier, 1996; England and Molnar, 1997; Holt et al., 2000]. The inability to decipher between these contrasting tectonic models is in large part due to insufficient kinematic constraints and the fact that the methods focus on the limited time span of the past 10s of years. Regarding the Altyn Tagh fault for example, the discrepancy between high slip rates determined from offset Quaternary features and low slip rates determined from GPS and paleoseismic studies may result from episodic deformation not integrated in time by the latter methods [Bendick et al., 2000; Meriaux et al., 2000; Washburn et al., 2001]. These issues raise concerns about whether recent deformation rates can be extrapolated back tens of millions of years to describe the evolution of the Himalaya-Tibetan orogen.

[4] A relatively unexplored aspect of the debate between distributed versus localized deformation models of Asia is their contrasting predictions on rates and distribution of vertical axis rotations. On the one hand, localized deformation models predict extrusion of large rigid blocks with rates of rotation approaching $\sim 1^\circ/\text{m.y.}$ (Figure 1a) [Molnar and Lyon-Caen, 1989; Avouac and Tapponnier, 1993; Peltzer and Saucier, 1996; England and Molnar, 1997]. On the other hand, distributed deformation models predict mainly crustal thickening with limited rotations except within distributed shear zones off the eastern and western edge of the Indian indenter and within the Altyn Tagh and Karakorum fault systems (Figure 1b) [England and Houseman, 1986; Cobbold and Davy, 1988; England and Molnar, 1990; Holt et al., 2000]. In principle, paleomagnetism can provide determination of the net rotation experienced since the age of the rocks analyzed. In turn this information is a powerful test of tectonic models. In this paper, we present paleomagnetic results from Cretaceous and Tertiary intermountain basin fill deposits adjacent to and south of the Altyn Tagh fault to quantitatively constrain Cenozoic vertical axis rotations and thereby test models for development of the Himalayan-Tibetan orogen.

[5] The Altyn Tagh fault (ATF), a major intracontinental left-lateral strike-slip fault, is a key element in the accommodation of deformation and possible extrusion of the Tibetan Plateau [Burchfiel et al., 1989; Meyer et al., 1998; Tapponnier et al., 2001]. The ATF forms the boundary between northern Tibet and the Tarim Basin (Figure 2). Along the north side of the ATF is a narrow zone of high elevation, the Altyn Tagh range. At the northeastern termination of the fault, sinistral strike-slip motion is transferred to compressional deformation within the Nan Shan fold-thrust belt. The low elevation Hexi Corridor in the foreland of the Nan Shan fold-thrust belt marks the boundary between the Tibetan Plateau and the Sino-Korean craton. Structural and tectonostratigraphic features can be correlated

from the Altyn Tagh range to the Nan Shan yielding estimates of left-lateral offset on the eastern part of the ATF in the 300–400 km range [Ritts and Biffi, 2000; Meng et al., 2001; Yue et al., 2001] with the most precise estimate at 280 ± 30 km [Yin and Harrison, 2000]. While Miocene rapid cooling is recorded in the Nan Shan and Altyn Tagh range [Jolivet et al., 1999; George et al., 2001; Sobel et al., 2001; Jolivet et al., 2002], crustal shortening prior to ca. 33 Ma is indicated by provenance and magnetostratigraphic analyses of synorogenic sediments [Yin et al., 2002]. These observations, consistent with the regional Cenozoic stratigraphy showing Early Oligocene to Quaternary coarsening upward sediments laying unconformably on basement rocks, suggest initiation of the ATF at least as early as Oligocene [Wang and Coward, 1990, 1993; Vincent and Allen, 1999; Yin et al., 2002].

[6] Previous paleomagnetic results provide important context for this study. Off the western and eastern edges of the Indian indenter, Cretaceous to Tertiary sediments yield vertical axis rotations in counterclockwise and clockwise sense respectively in agreement with most tectonic models [Lin and Watts, 1988; Otofuji et al., 1990; Huang et al., 1992; Thomas et al., 1993, 1994; Geissman et al., 2001]. Within the center of the orogen, paleomagnetic data available from Cretaceous to Tertiary red beds in the Tarim Basin indicate no significant vertical axis rotations [see Dupont-Nivet et al., 2002b, and references therein]. Similarly, no Neogene vertical axis rotations of the Qaidam Basin are indicated by paleomagnetic results from Oligocene to Pliocene sediments from the interior of the basin at two locations separated by several hundred kilometers [Dupont-Nivet et al., 2002a]. Deformation concentrated on the ATF rather than distributed away from the fault is suggested by paleomagnetic results near Tula, a few tens of kilometers south of the ATF [Robinson et al., 2002b; Dupont-Nivet et al., 2003]. Concordant paleomagnetic directions recorded along the arcuate shape of the Tula uplift indicates the absence of oroclinal bending by shear distributed south of the ATF (Figure 3a). However, based on different paleomagnetic results, Chen et al. [2002a] have recently concluded that the Qaidam Basin experienced $>20^\circ$ clockwise rotation during the Neogene resulting in differential shortening in the Nan Shan fold-thrust belt (Figure 3b). The predicted differential shortening would imply clockwise rotations within the Nan Shan fold-thrust belt in apparent agreement with 20° – 30° clockwise rotations observed in paleomagnetic data from Early Cretaceous rocks in the Hexi corridor and the Xining-Lanzhou basin [Frost et al., 1995; Halim et al., 1998; Yang et al., 2002]. However, paleomagnetic data from Early Cretaceous red beds north of the Hexi corridor showing no vertical axis rotation cast doubts on these early interpretations [Chen et al., 2002b]. To clarify the vertical axis rotation pattern in northern Tibet, we collected over 1200 paleomagnetic samples from 153 sites in Cretaceous to Tertiary red sedimentary rocks at seven paleomagnetic localities in the Altyn Tagh range, the Nan Shan fold-thrust belt and the Hexi corridor.

2. Methods

[7] Paleomagnetic sampling was performed using methods referenced by Butler [1992]. At each site (i.e., sedimentary

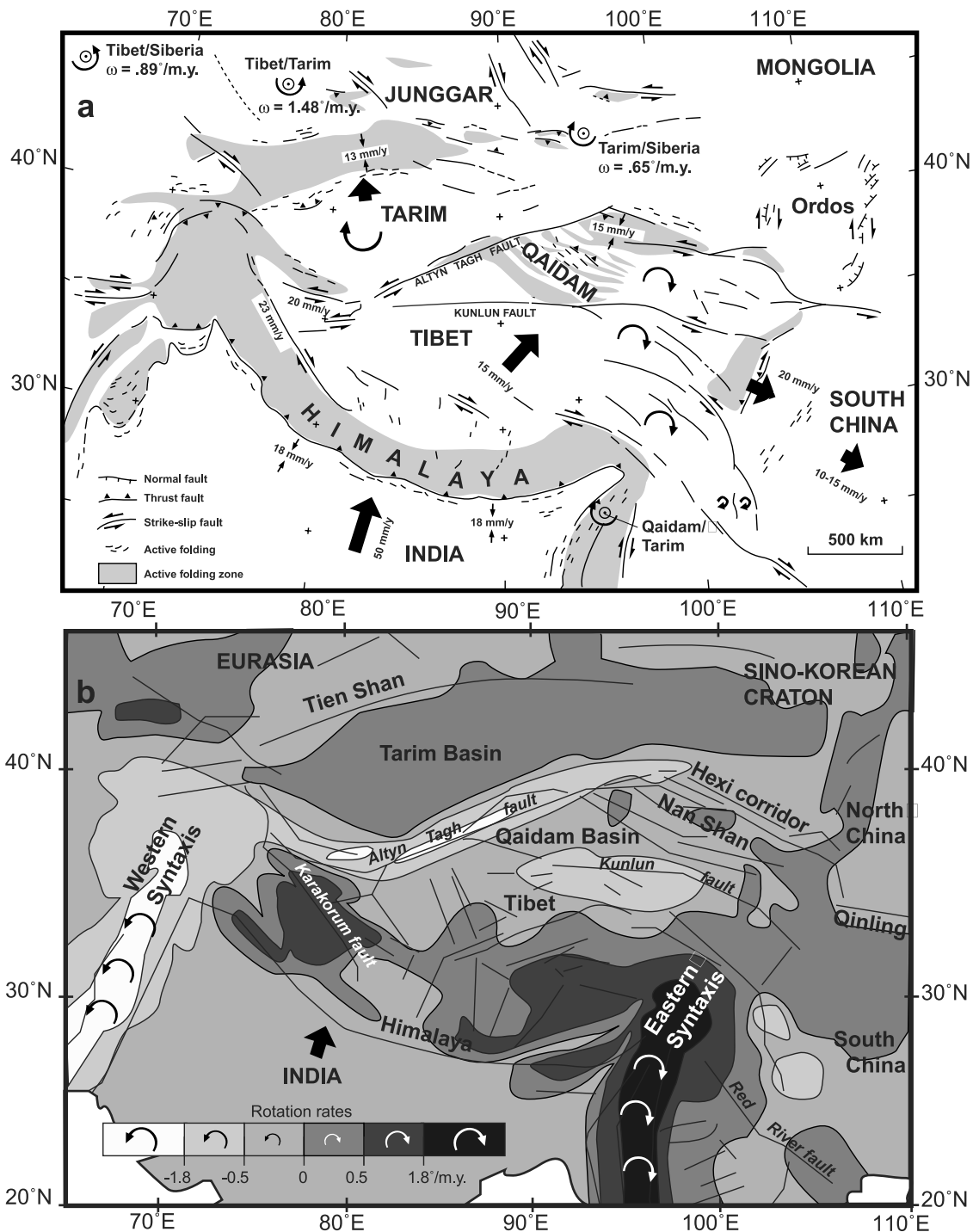


Figure 1. Expected vertical axis rotations for central Asia. (a) Model developed assuming rigid block deformation and based on inversion of Quaternary fault slip rates [after *Avouac and Tapponnier, 1993; Chen et al., 2002a*]. (b) Model resulting from deformation distributed over a continuum and based on the combined inversion of Quaternary fault slip rates, GPS and VLBI observations [after *Holt et al., 2000*].

horizon), eight oriented core samples were collected and bedding attitude was measured. When variations in bedding attitude were minor, several sites were collected from a continuously exposed section and a section-mean bedding attitude was calculated. We apply the term paleomagnetic locality to an area (usually with dimensions <10 km) from which one or several stratigraphic sections were sampled. All samples were stored, thermally demagnetized and measured

in a magnetically shielded room with average field intensity below 200 nT. After initial measurement of natural remanent magnetization (NRM), samples were thermally demagnetized at 10 to 20 temperatures from 50°C to 700°C. Results from at least four successive temperatures were analyzed by principal component analysis [Kirschvink, 1980] to determine sample characteristic remanent magnetization (ChRM) directions. Samples yielding maximum angular deviation

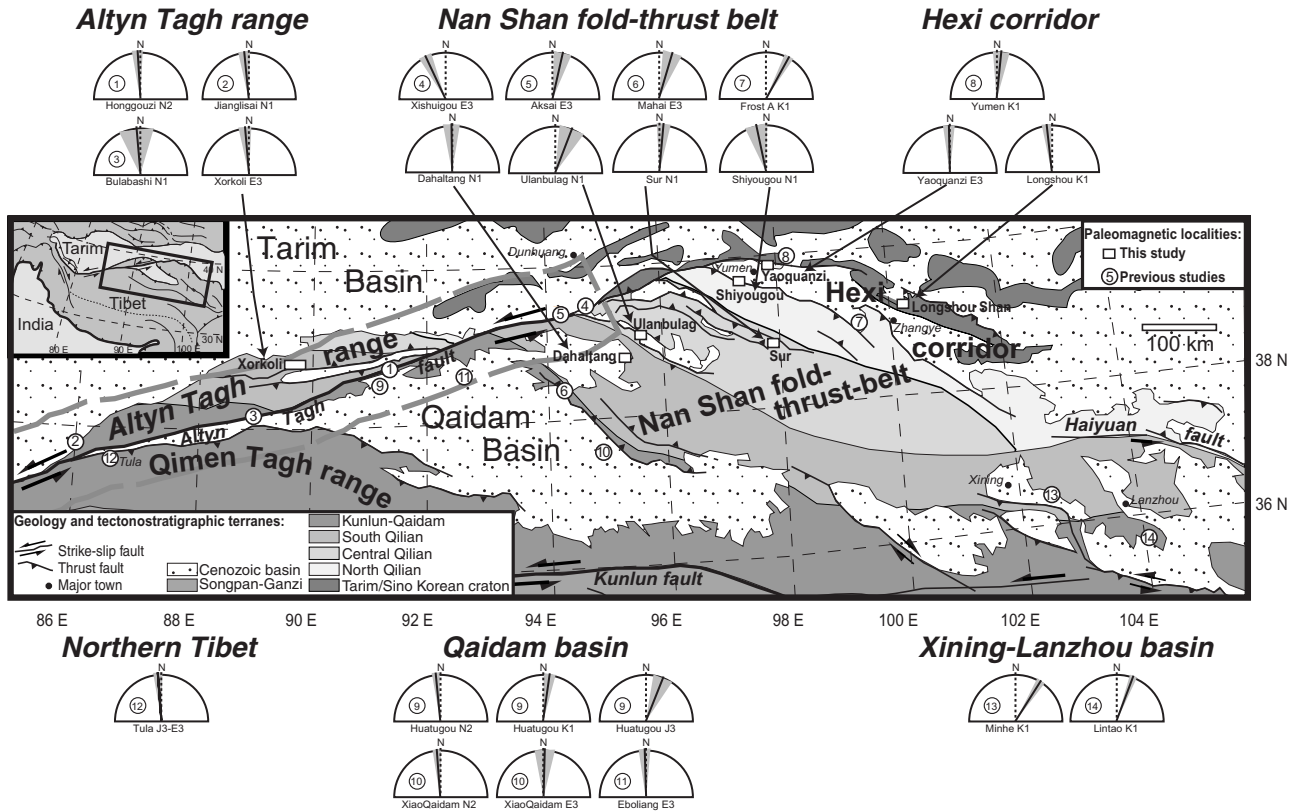


Figure 2. General tectonic map of the northeastern Tibetan Plateau showing major structures, geologic terranes, and Cenozoic basins [Yin and Harrison, 2000]. Inset at top left corner shows location with elevations over 2000 m shaded. Paleomagnetic sampling localities of this study are labeled and indicated by boxes. Sampling localities from previous studies are indicated by circles with numbers referenced in Table 1. Vertical axis rotations with 95° confidence limits are illustrated for each locality. Arrows pointing to sampling locality are given for results from this study. Cenozoic rotations for localities within 60 km from the Alтын Tagh fault (dashed gray box) are plotted on Figure 12.

(MAD) >15° were rejected from further analysis. Site-mean ChRM directions were calculated using methods of Fisher [1953]. Sample ChRM directions more than two angular standard deviations from the initial site-mean direction were rejected prior to final site-mean calculation. Sites with less than four sample ChRM directions and site-mean directions with $\alpha_{95} > 25^\circ$ were rejected. Locality-mean directions were calculated by applying Fisher [1953] statistics to the set of normal-polarity site-mean directions and antipodes of reversed-polarity site-mean directions from each locality (discarding site means more than two angular standard deviations from the preliminary mean). The expected direction at a paleomagnetic locality was calculated using the appropriate age reference paleomagnetic pole for Eurasia from Besse and Courtillot [2002]. Concordance/discordance calculations followed the methods of Beck [1980] and Demarest [1983] (Table 1).

3. Results

3.1. Xorkoli Valley in Alтын Tagh Range

[8] In the Eastern Alтын Tagh range, 44 sites were collected in four gently dipping stratigraphic sections of red sedimentary rocks from the northern Xorkoli basin

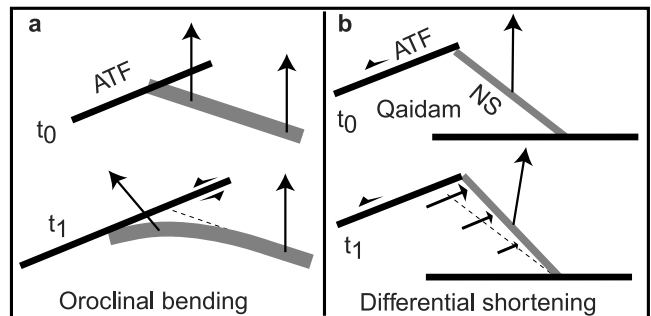


Figure 3. (a) Oroclinal bending model. ATF is Alтын Tagh fault system. Arrows indicate paleomagnetic declination before (t_0) and after (t_1) motion on the ATF. At t_1 , the dotted line indicates the original position of the arcuate feature before oroclinal bending. (b) Differential shortening mechanism. Arrows indicate paleomagnetic declination before (t_0) and after (t_1) motion on the ATF. At t_1 , the dotted line shows the original position of the rotated feature before differential shortening within the Nan Shan fold-thrust belt as indicated by arrows of decreasing length.

Table 1. Locality Paleomagnetic Directions Compared to Expected Directions^a

| Locality | Reference | Age | Location | | | Observed direction | | | Reference Pole | | | Rotation, deg | | Flattening, deg | |
|----------------------------------|------------------------------------|--------------------------------|----------|---------|------|--------------------|--------------|-------------------|----------------|--------|---------|----------------|------------|-----------------|------------|
| | | | Lat °N | Long °E | | <i>I</i> deg | <i>D</i> deg | α_{95} deg | Sites <i>N</i> | Lat °N | Long °E | A_{95} , deg | <i>R</i> , | $\pm\Delta R$ | <i>F</i> |
| Honggouzi (1) | <i>Chen et al.</i> [2002a] | N ₂ | 38.68 | 91.10 | 54.5 | 1.3 | 4.4 | 10 | 86.3 | 172.0 | 2.6 | -3.4 | ± 6.6 | 4.0 | ± 4.0 |
| Jianglisa (2) | <i>Rumelhart et al.</i> [1999] | N ₁ | 38.00 | 86.50 | 39.6 | 358.4 | 6.7 | 28m | 84.2 | 155.3 | 1.9 | -5.5 | ± 7.2 | 19.5 | ± 5.5 |
| Bulabashi (3) | <i>Chen et al.</i> [2002a] | N ₁ | 38.16 | 88.70 | 37.6 | 2.1 | 20.7 | 3 | 84.2 | 155.3 | 1.9 | -4.9 | ± 21.3 | 21.8 | ± 16.6 |
| Xorkoli | this study | E ₃ | 38.93 | 91.43 | 49.7 | 5.0 | 5.4 | 21 | 82.4 | 171.7 | 3.7 | -4.8 | ± 7.7 | 9.5 | ± 5.1 |
| <i>Alayn Tagh Range</i> | | | | | | | | | | | | | | | |
| <i>Nan Shan Fold-Thrust Belt</i> | | | | | | | | | | | | | | | |
| Dahatang | this study | N ₁ | 38.77 | 95.53 | 46.7 | 5.7 | 8.9 | 12 | 84.2 | 155.3 | 1.9 | -1.0 | ± 10.6 | 13.8 | ± 7.2 |
| Ulanbulag | this study | N ₁ | 39.03 | 95.72 | 38.5 | 28.3 | 14.4 | 5 | 84.2 | 155.3 | 1.9 | 21.6 | ± 15.0 | 22.3 | ± 11.6 |
| Sur | this study | N ₁ | 38.73 | 97.97 | 30.0 | 11.6 | 8.8 | 10 | 84.2 | 155.3 | 1.9 | 5.1 | ± 8.4 | 30.7 | ± 7.2 |
| Shiyogou | this study | N ₁ | 39.69 | 97.66 | 41.3 | 358.4 | 12.4 | 12 | 84.2 | 155.3 | 1.9 | -8.3 | ± 13.4 | 20.2 | ± 10 |
| Mean (localities) | this study | N ₁ | 39.06 | 96.72 | 40.0 | 11.4 | 13.8 | 4 | 84.2 | 155.3 | 1.9 | 4.8 | ± 14.7 | 20.9 | ± 11.1 |
| Mean (sites) | this study | N ₁ | 39.06 | 96.72 | 40.6 | 7.2 | 5.8 | 39 | 84.2 | 155.3 | 1.9 | 0.6 | ± 6.5 | 20.3 | ± 4.8 |
| Xishuigou (4) | <i>Rumelhart et al.</i> [1999] | E ₃ | 39.50 | 94.80 | 39.7 | 344.7 | 6.6 | 76 m | 82.4 | 171.7 | 3.7 | -25.1 | ± 7.9 | 20.2 | ± 5.9 |
| Aksai (5) | <i>Chen et al.</i> [2002a] | E ₃ | 39.20 | 94.30 | 38.2 | 22.5 | 9.7 | 6 | 82.4 | 171.7 | 3.7 | 12.7 | ± 10.6 | 21.4 | ± 8.2 |
| Mahai (6) | <i>Chen et al.</i> [2002a] | E ₃ | 38.40 | 94.30 | 40.0 | 26.2 | 10.5 | 7 | 82.4 | 171.7 | 3.7 | 16.5 | ± 11.7 | 18.9 | ± 8.8 |
| Frost A (7) | <i>Frost et al.</i> [1995] | K ₁ | 39.00 | 99.60 | 39.0 | 41.9 | 5.1 | 16 s | 79.8 | 188.0 | 2.5 | 28.8 | ± 5.8 | 18.9 | ± 4.5 |
| <i>Hexi Corridor</i> | | | | | | | | | | | | | | | |
| Yaoquanzi | this study | E ₃ | 39.97 | 97.68 | 33.0 | 8.6 | 6.0 | 12 | 82.4 | 171.7 | 3.7 | -1.2 | ± 7.0 | 27.7 | ± 5.4 |
| Longshou | this study | K ₁ | 39.09 | 100.50 | 53.4 | 6.8 | 3.8 | 36 | 79.8 | 188.0 | 2.5 | -6.3 | ± 5.7 | 4.7 | ± 3.6 |
| Yumen (8) | <i>Chen et al.</i> [2002b] | K ₁ | 39.90 | 97.70 | 61.7 | 18.9 | 5.7 | 9 | 79.8 | 188.0 | 2.5 | 5.7 | ± 10.0 | -3.3 | ± 4.9 |
| <i>Qaidam Basin</i> | | | | | | | | | | | | | | | |
| Huatugou (9) | <i>Chen et al.</i> [2002a] | N ₂ | 38.35 | 90.90 | 46.9 | 359.2 | 3.3 | 19 | 86.3 | 172.0 | 2.6 | -5.5 | ± 4.7 | 11.3 | ± 3.3 |
| Huatugou (9) | <i>Chen et al.</i> [2002a] | K ₁ | 38.44 | 90.73 | 36.7 | 20.7 | 6.7 | 5 | 79.8 | 188.0 | 2.5 | 8.1 | ± 7.1 | 19.2 | ± 5.7 |
| Huatugou (9) | <i>Chen et al.</i> [2002a] | J ₃ | 37.46 | 90.75 | 34.8 | 40.4 | 7.5 | 9 | 75.4 | 175.5 | 9.6 | 21.7 | ± 12.2 | 22.9 | ± 9.3 |
| XiaoQaidam (10) | <i>Dupont-Nivet et al.</i> [2002a] | N ₂ | 37.40 | 95.30 | 48.6 | 0.4 | 3.6 | 30 | 86.3 | 172.0 | 2.6 | -4.2 | ± 5.1 | 8.9 | ± 3.5 |
| XiaoQaidam (10) | <i>Dupont-Nivet et al.</i> [2002a] | E ₃ | 37.50 | 95.20 | 37.3 | 11.0 | 11.5 | 6 | 82.4 | 171.7 | 3.7 | 1.5 | ± 12.2 | 20.9 | ± 9.6 |
| Eboliang (11) | <i>Dupont-Nivet et al.</i> [2002a] | E ₃ | 38.70 | 92.80 | 43.6 | 8.0 | 5.1 | 16 | 82.4 | 171.7 | 3.7 | -1.7 | ± 6.8 | 15.4 | ± 4.9 |
| <i>Northern Tibet</i> | | | | | | | | | | | | | | | |
| Tula (12) | <i>Dupont-Nivet et al.</i> [2003] | J ₃ -E ₃ | 37.50 | 95.20 | 28.6 | 8.3 | 5.5 | 41 | 79.8 | 190.2 | 2.3 | -4.3 | ± 5.5 | 26.8 | ± 4.8 |
| <i>Xining-Lanzhou Basin</i> | | | | | | | | | | | | | | | |
| Minhe (13) | <i>Halim et al.</i> [1998] | K ₁ | 36.20 | 103.50 | 43.7 | 45.0 | 4.3 | 9 | 79.8 | 188.0 | 2.5 | 32.3 | ± 5.4 | 12.3 | ± 3.9 |
| Lintao (14) | <i>Yang et al.</i> [2002] | K ₁ | 35.80 | 103.80 | 50.3 | 33.2 | 3.0 | 19 | 79.8 | 188.0 | 2.5 | 20.6 | ± 4.5 | 5.3 | ± 3.1 |

^aLocality, name of paleomagnetic sampling locality; for previous studies, numbers are keyed to label location on Figure 2. Age, geological age of sampled formations: J₃, Late Jurassic; K₁, Early Cretaceous; E₃, Oligocene; N₁, Miocene; N₂, Pliocene. Location, Lat and Long, latitude and longitude of sampling locality. Observed direction mean paleomagnetic direction: *I* and *D*, inclination and declination in stratigraphic coordinates with α_{95} radius of 95% confidence circle. Sites *N*, number of sites used to calculate mean direction (m if includes magnetostratigraphic sites; s if mean of individual sample directions). Reference pole, Lat, Long, A_{95} , latitude, longitude, 95% confidence limit of Eurasian paleomagnetic pole [*Besse and Courtillot*, 2002]. Rotation, $R \pm \Delta R$, vertical axis rotation with 95% confidence limit (positive indicates clockwise rotation). Flattening $F \pm \Delta F$, flattening of inclination with 95% confidence limit. Rotation and flattening are derived from observed direction minus expected direction at locality calculated from reference pole.

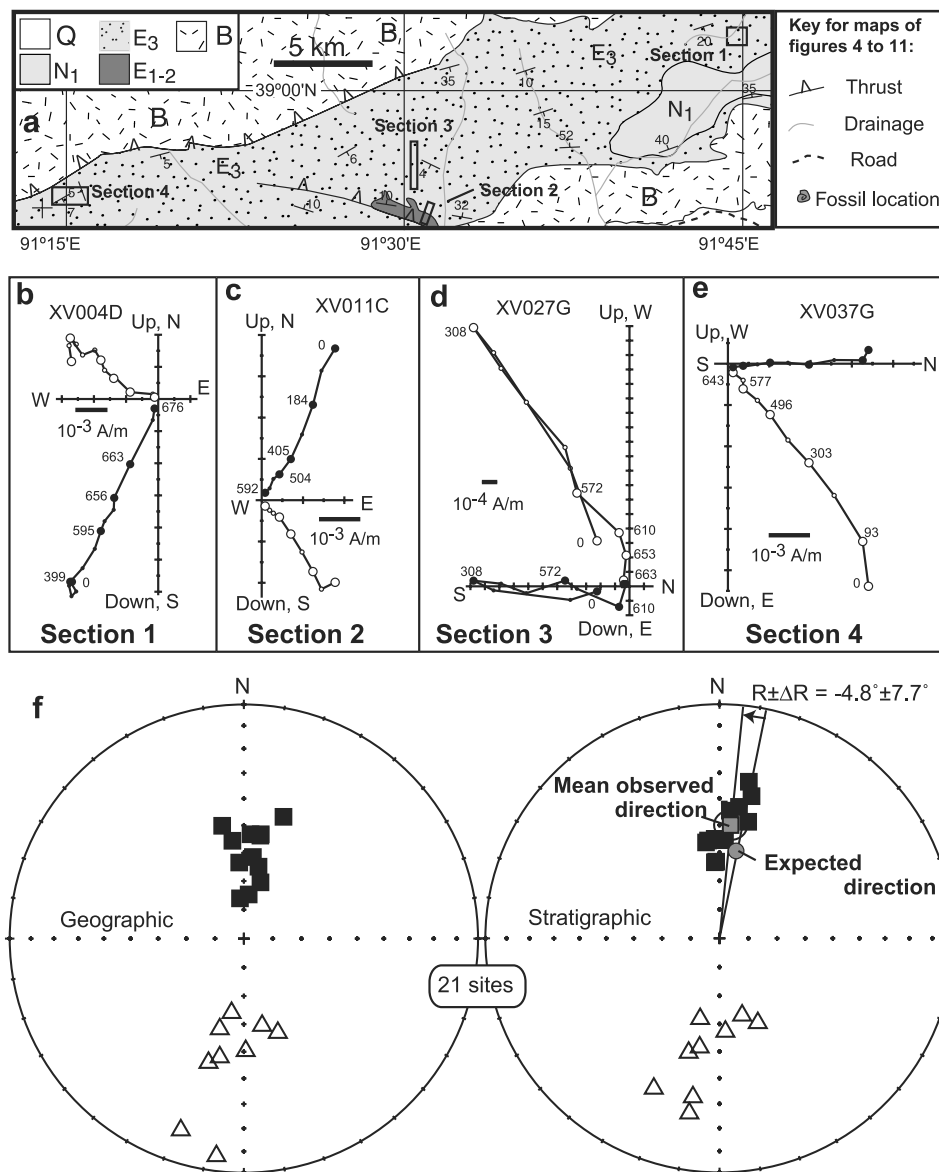


Figure 4. Xorkoli paleomagnetic locality. (a) Geologic map in vicinity of sampled sections shown by boxes. Abbreviation for formation ages on maps of Figures 4 through 11 are Q, Quaternary; N_2 , late Miocene; N_1 , early Miocene; E_3 , Oligocene; E_{1-2} , Paleocene-Eocene; K, Cretaceous; B, undifferentiated basement rock. (b), (c), (d), (e) Vector endpoint diagrams in geographic coordinates for typical samples from different sections. Solid circles are projection on the horizontal plane, and open circles are projection on the vertical plane. Numbers adjacent to data points indicate temperature in $^{\circ}\text{C}$. (f) Equal-area projection of site-mean ChRM directions in geographic and stratigraphic coordinates. Solid squares are in lower hemisphere, and open triangles are in upper hemisphere. In stratigraphic coordinates, the gray square indicates the locality-mean direction, and gray circle is the expected direction calculated from the Oligocene paleomagnetic pole of Eurasia.

(Figures 2 and 4a). Paleomagnetic samples were taken from fine-grained sandstone to mudstone horizons within a thick formation of sandy-conglomerate interlayered with sandstone, mudstone and gypsum. Sampled sections belong to the Lower Gancaigou Formation (E_{3g}) assigned an Oligocene age based on stratigraphic correlation to nearby sections yielding fossil assemblages (*Ilipocris* cf. *errabundis*; *Condoniella marcida*, *Eucypris* sp.; *Sphaerium* cf.

rivicolum; map J-46-VIII, scale 1:200,000 [Xinjiang Bureau of Geological and Mineral Resources (XBGRM), 1993; Yue et al., 2001]).

[9] Two pilot samples from each site were demagnetized using 20 temperature steps up to 700°C . For pilot samples from 20 Xorkoli Valley sites, a low intensity NRM (below 10^{-4} A/m) was completely demagnetized below 450°C and erratic demagnetization paths prevented determination

Table 2. Site-Mean Directions From the Xorkoli Paleomagnetic Locality^a

| Sites | Lat °N | Long °E | Geographic | | Stratigraphic | | α_{95} , deg | k | n/N | Dip, deg | Dip Az, deg |
|--------------------|--------|---------|------------|-----------|---------------|-----------|---------------------|-------|-------|----------|-------------|
| | | | I , deg | D , deg | I , deg | D , deg | | | | | |
| <i>Section 1</i> | | | | | | | | | | | |
| XV003 | 39.03 | 91.75 | -7.1 | 187.2 | -25.1 | 189.8 | 16.4 | 24.3 | 4/5 | 20.0 | 162.0 |
| XV004 | 39.03 | 91.75 | -14.9 | 198.2 | -30.6 | 203.6 | 10.0 | 38.3 | 6/6 | 20.0 | 162.0 |
| <i>Section 2</i> | | | | | | | | | | | |
| XV011 | 38.92 | 91.52 | 74.6 | 6.2 | 42.7 | 8.4 | 11.0 | 26.8 | 7/7 | 31.9 | 9.7 |
| XV012 | 38.92 | 91.52 | 76.0 | 354.5 | 44.5 | 4.6 | 12.4 | 21.0 | 7/7 | 31.9 | 9.7 |
| XV013 | 38.92 | 91.52 | 64.4 | 11.5 | 32.5 | 10.6 | 10.7 | 33.3 | 6/7 | 31.9 | 9.7 |
| XV014 | 38.92 | 91.52 | 69.6 | 16.5 | 37.8 | 12.7 | 12.7 | 38.3 | 4/5 | 31.9 | 9.7 |
| XV020 ^b | 38.92 | 91.52 | 29.4 | 330.5 | 3.4 | 336.3 | 13.8 | 47.1 | 4/4 | 31.9 | 9.7 |
| XV022 ^b | 38.92 | 91.52 | -40.3 | 137.4 | -17.6 | 150.4 | 19.5 | 44.8 | 3/5 | 31.9 | 9.7 |
| XV025 | 38.92 | 91.52 | -63.7 | 189.4 | -31.8 | 189.5 | 11.4 | 36.9 | 5/6 | 31.9 | 9.7 |
| <i>Section 3</i> | | | | | | | | | | | |
| XV027 | 38.93 | 91.50 | -58.8 | 168.2 | -61.9 | 163.7 | 7.9 | 75.6 | 5/5 | 4.0 | 206.0 |
| XV028 | 38.93 | 91.50 | -57.1 | 194.9 | -61.0 | 193.5 | 13.8 | 34.2 | 4/4 | 4.0 | 206.0 |
| XV029 | 38.93 | 91.50 | -47.1 | 191.5 | -50.9 | 190.3 | 4.8 | 138.4 | 7/7 | 4.0 | 206.0 |
| XV030 | 38.93 | 91.50 | -50.3 | 179.1 | -57.2 | 176.4 | 2.7 | 357.2 | 8/8 | 4.0 | 206.0 |
| XV031 | 38.93 | 91.50 | -44.1 | 195.9 | -48.1 | 195.1 | 7.8 | 44.9 | 8/8 | 4.0 | 206.0 |
| XV034 | 38.93 | 91.50 | -54.8 | 160.2 | -57.4 | 155.7 | 17.3 | 16.3 | 5/5 | 4.0 | 206.0 |
| <i>Section 4</i> | | | | | | | | | | | |
| XV035 | 38.93 | 91.25 | 44.5 | 18.0 | 47.5 | 13.8 | 15.6 | 26.7 | 4/4 | 5.0 | 250.0 |
| XV036 | 38.93 | 91.25 | 61.3 | 6.3 | 63.2 | 357.5 | 4.9 | 110.8 | 8/8 | 5.0 | 250.0 |
| XV037 | 38.93 | 91.25 | 53.2 | 3.7 | 55.0 | 357.2 | 4.1 | 187.7 | 7/7 | 5.0 | 250.0 |
| XV038 | 38.93 | 91.25 | 53.3 | 9.1 | 55.5 | 2.8 | 5.3 | 135.4 | 6/8 | 5.0 | 250.0 |
| XV039 | 38.93 | 91.25 | 52.8 | 9.2 | 55.0 | 3.1 | 6.3 | 68.3 | 8/8 | 5.0 | 250.0 |
| XV040 | 38.93 | 91.23 | 63.4 | 356.5 | 63.4 | 356.5 | 5.7 | 146.0 | 5/5 | 0.0 | 0.0 |
| XV041 | 38.93 | 91.23 | 55.4 | 353.3 | 55.4 | 353.3 | 5.3 | 132.8 | 6/6 | 0.0 | 0.0 |
| XV043 ^b | 38.92 | 91.25 | 44.7 | 50.9 | 45.6 | 57.9 | 11.6 | 48.0 | 4/4 | 7.0 | 152.0 |
| XV044 | 38.92 | 91.25 | 49.4 | 349.1 | 56.0 | 352.0 | 18.8 | 18.7 | 4/6 | 7.0 | 152.0 |
| Mean | 38.93 | 91.43 | 53.9 | 5.5 | | | 7.0 | 21.4 | 21/24 | | |
| Mean | 38.93 | 91.43 | | | 49.7 | 5.0 | 5.4 | 35.3 | 21/24 | | |

^aSites, paleomagnetic site number; Lat and Long, latitude and longitude of site; geographic and stratigraphic I and D , inclination and declination of site-mean direction in geographic coordinates (with no structural correction) and stratigraphic coordinates (after restoration of local bedding to horizontal); α_{95} , radius of cone of 95% confidence about site-mean direction; k , concentration parameter; n/N , number of sample ChRM directions averaged to calculate site-mean paleomagnetic direction/number of sample ChRM directions determined from the site; dip, angle of dip of local bedding; dip az, azimuth of downdip direction of local bedding; mean, average direction for locality calculated by treating each site-mean direction as a unit vector is given in stratigraphic and geographic coordinates.

^bSite-mean direction discarded from calculation of the overall locality-mean direction.

of ChRM directions. These sites were discarded from further analysis. For pilot samples from the remaining 24 sites, demagnetization of stronger intensity NRM (above 10^{-3} A/m) yielded interpretable ChRM directions and thermal demagnetization of the remaining samples was undertaken. ChRM unblocking temperatures predominantly below 600°C suggest that magnetite is the dominant ferrimagnetic mineral in samples from sections 2 and 4 (Figures 4c and 4e). ChRM carried entirely by hematite or by a combination of magnetite and hematite is suggested by unblocking temperatures of samples from sections 1 and 3 (Figures 4b and 4d). Occasional secondary components of NRM were removed below 300°C (Figure 4d). From the 24 site-mean ChRM directions listed in Table 2, three outlying directions were discarded. The final 21 site-mean directions form antipodal normal- and reversed-polarity clusters (Figure 4f). The *Watson and Enkin* [1993] fold test is positive with 95% confidence when applied to the six mean ChRM directions of the limbs defined by the six different bedding attitudes from which the sites were sampled. A positive Class C reversal test further suggests that the ChRM is a primary magnetization [McFadden and McElhinny, 1990]. The locality-mean

direction has a concordant declination and slightly shallow inclination compared to the expected Oligocene direction (Figure 4f and Table 1). The origin of shallow paleomagnetic inclinations in Cenozoic red sedimentary rocks of Asia is a complex subject of some debate. As explained by *Dupont-Nivet et al.* [2002b], we suspect depositional and/or postdepositional rock magnetic effects are responsible for the shallow inclinations.

3.2. Nan Shan Fold-Thrust Belt

[10] Paleomagnetic sampling was done along a southwest to northeast transect through the South, Central, and North Qilian terranes of the Nan Shan fold-thrust belt (Figure 2). Interpretable results were obtained at four localities and are presented below progressing from southwest to northeast across the Nan Shan. Results from two localities that did not yield interpretable ChRM are also presented.

3.2.1. Dahaltang

[11] This paleomagnetic locality is on the southwest side of the Dang He Nan Shan within the South Qilian terrane (Figure 2). Near a notable hairpin shaped bend of the Dahaltang river (Figure 5a), samples were collected from 16 sites in a continuously exposed 80-m-thick section of fine

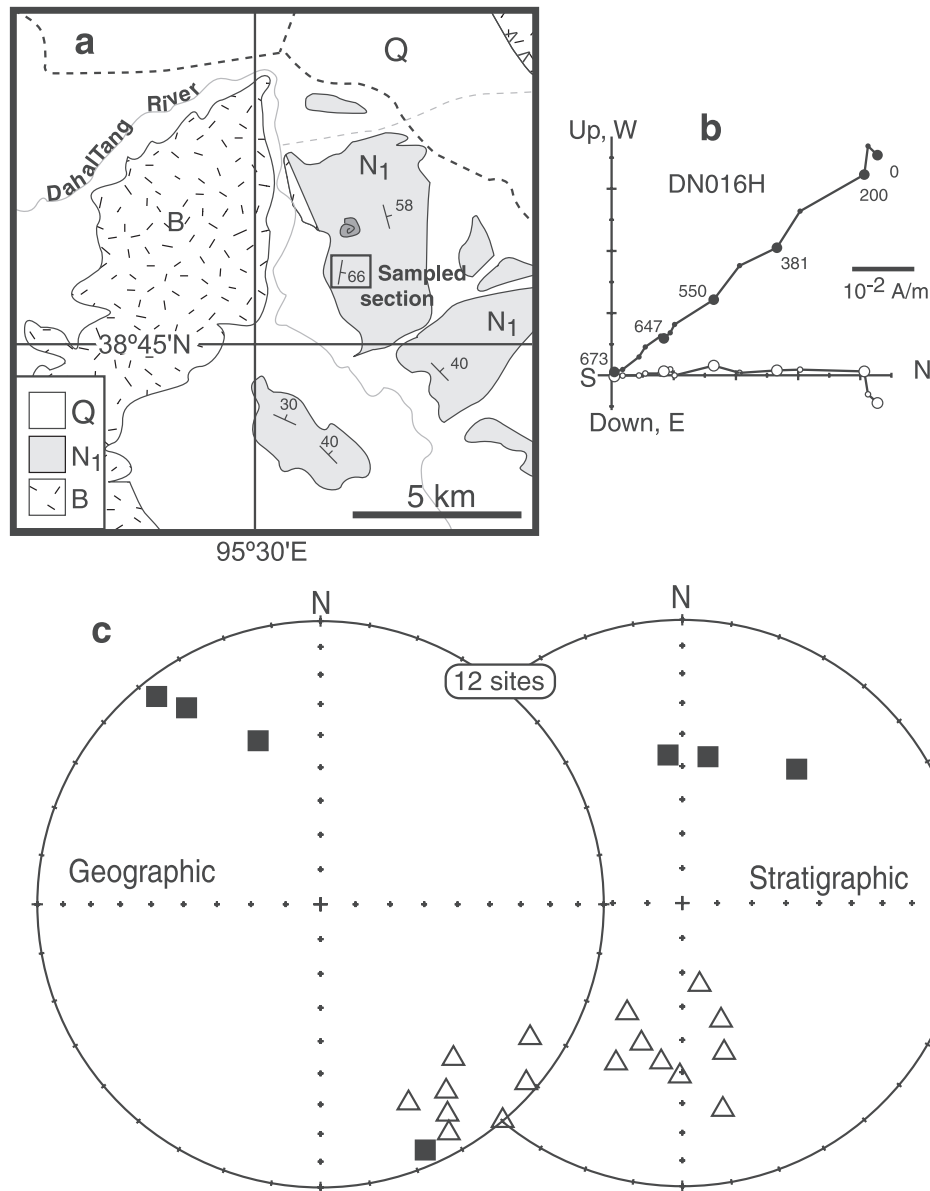


Figure 5. Dahaltang paleomagnetic locality of the Nan Shan fold-thrust belt. (a) Geologic map in vicinity of sampled section shown by box. (b) Vector endpoint diagram of typical sample in geographic coordinates. (c) Equal-area projection of site-mean ChRM directions in geographic and stratigraphic coordinates. Symbols are as in Figure 4.

sandstone and mudstone. The sampled strata belong to a formation described as conglomeratic with brown intercalated claystone and siltstone. On the basis of fossil occurrences (*Planorbis cf. youngi*), these rocks are assigned a Miocene (N_1) age (Figure 5a, map J-46-XII, scale 1:200,000 [Qinghai Bureau of Geology and Mineral Resources, 1991]).

[12] Upon thermal demagnetization, 13 sites yielded interpretable ChRM directions. Samples from these sites show relatively high NRM intensity (above 10^{-2} A/m). Unblocking temperatures dominantly in the 200°C – 600°C range but extending into the 650°C – 690°C range indicate that ChRM is carried by a combination of magnetite and hematite (Figure 5b). One site-mean direction with $\alpha_{95} > 25^{\circ}$ was rejected. As illustrated in Figure 5c and Table 3, antipodal normal- and reverse-polarity groupings of the

remaining 12 site-mean directions pass the reversal test with class C [McFadden and McElhinny, 1990]. Bedding attitude is uniform through the section so a local fold test is not possible. Results of regional field tests are reported below and suggest a primary origin for the ChRM.

3.2.2. Ulanbulag

[13] This paleomagnetic locality is on the northern flank of the Dang He Nan Shan within the Central Qilian terrane (Figure 2). In the valley of the Dang He river, a suitable section gently dipping to the southwest was found ~ 10 km to the west of the village of Ulanbulag (Figure 6a). It is composed of conglomerate with intercalated fine-grained siltstone, mudstone and occasional gypsum layers. Thirty paleomagnetic sites covering 150 m of stratigraphic thickness were collected from beds of fine-grained brick-red

Table 3. Site-Mean Directions From the Dahaltang Paleomagnetic Locality^a

| Sites | Lat °N | Long °E | Geographic | | Stratigraphic | | α_{95} deg | <i>k</i> | <i>n/N</i> | Dip, deg | Dip Az., deg |
|-------|--------|---------|----------------|----------------|----------------|----------------|-------------------|----------|------------|----------|--------------|
| | | | <i>I</i> , deg | <i>D</i> , deg | <i>I</i> , deg | <i>D</i> , deg | | | | | |
| DN001 | 38.77 | 95.53 | -28.9 | 139.3 | -54.2 | 206.6 | 17.2 | 29.5 | 4/4 | 66.3 | 99.6 |
| DN002 | 38.77 | 95.53 | -24.2 | 156.2 | -38.7 | 202.5 | 9.9 | 27.8 | 9/9 | 66.3 | 99.6 |
| DN004 | 38.77 | 95.53 | -13.3 | 122.5 | -65.9 | 168.0 | 16.2 | 23.3 | 5/5 | 66.3 | 99.6 |
| DN005 | 38.77 | 95.53 | -21.5 | 146.1 | -47.2 | 196.2 | 10.5 | 28.8 | 8/8 | 66.3 | 99.6 |
| DN006 | 38.77 | 95.53 | -4.3 | 131.0 | -54.0 | 161.8 | 10.8 | 31.9 | 7/8 | 66.3 | 99.6 |
| DN007 | 38.77 | 95.53 | -14.4 | 148.9 | -42.7 | 187.6 | 6.8 | 67.7 | 8/8 | 66.3 | 99.6 |
| DN008 | 38.77 | 95.53 | 6.3 | 156.9 | -26.6 | 168.9 | 13.9 | 16.8 | 8/8 | 66.3 | 99.6 |
| DN009 | 38.77 | 95.53 | 17.2 | 325.7 | 46.5 | 9.9 | 10.8 | 27.3 | 8/8 | 66.3 | 99.6 |
| DN010 | 38.77 | 95.53 | 38.2 | 339.1 | 37.9 | 40.5 | 8.3 | 45.2 | 8/8 | 66.3 | 99.6 |
| DN011 | 38.77 | 95.53 | -8.2 | 150.7 | -38.8 | 180.8 | 13.7 | 45.8 | 4/4 | 66.3 | 99.6 |
| DN012 | 38.77 | 95.53 | -0.1 | 139.9 | -44.4 | 164.4 | 8.0 | 71.4 | 6/7 | 66.3 | 99.6 |
| DN016 | 38.77 | 95.53 | 7.3 | 321.7 | 46.4 | 354.5 | 9.5 | 41.6 | 7/7 | 66.3 | 99.6 |
| Mean | 38.77 | 95.53 | 14.5 | 324.6 | 46.7 | 5.7 | 8.9 | 24.9 | 12/13 | | |

^aSee notes for Table 2.

sandstone. Although no fossils are reported from the sampled section, these strata are correlated with those sampled at Dahaltang and are therefore assigned a Miocene (N_1) age [Qinghai Bureau of Geology and Mineral Resources, 1991].

[14] All samples from this locality were thermally demagnetized. The majority of the samples from 24 sites had low intensity NRM (below 10^{-4} A/m) that was completely demagnetized below 450°C. No reliable ChRM directions could be determined from these sites. In the remaining six sites, a ChRM component was isolated by thermal demagnetization above 650°C suggesting a hematite carrier (Figure 6b). Although ChRM directions are well clustered within each site (Table 4), one outlying site-mean direction was discarded. Following structural correction, the five remaining sites pass the fold test at 99% significance [McFadden, 1990] showing a grouping of reversed-polarity site-mean directions that is roughly antipodal to the single normal-polarity site-mean direction (Figure 6c). However, the *McFadden and McElhinny* [1990] formulation of the reversal test is indeterminate. A primary origin for the ChRM at the Ulanbulag locality is confirmed by results of the regional field tests reported below.

3.2.3. Sur

[15] In the Central Qilian terrane, on the northeastern flank of the Shule Nan Shan (Figure 2), suitable outcrop was found across the river from the village of Sur (Figure 7a). Twelve sites were collected from brown sandy mudstones in a 30-m-thick homoclinal section of a Miocene formation (Figure 7a, map J-47-VIII [Qinghai Bureau of Geology and Mineral Resources, 1991]). For 10 sites, ChRM was isolated over a large range of unblocking temperatures suggesting that both magnetite and hematite are carriers of NRM (Figure 7b). Site-mean directions (Table 5 and Figure 7c) have positive inclinations and north to north-northeast declinations. Because all sites are normal polarity and there is no variation in bedding attitude, neither fold nor reversals tests can be applied. The likely primary origin of the ChRM is evidenced by the regional field test reported below.

3.2.4. Shiyougou

[16] The Shiyougou oil field is located in a piggyback basin at the northeast corner of the North Qilian terrane southwest of the town of Yumen (Figures 2 and 8a). Twenty-six sites were collected in brick-red mudstones and fine sandstones interbedded with the red sandstones of the 500-m-thick Miocene (N_{1b}) Baiyanghe Formation

(map J-47-II, scale 1:200,000 [Gansu Bureau of Geology and Mineral Resources, 1989]). Samples were collected from two sections. Section 1 comprises 14 sites covering a 130 m stratigraphic thickness; section 2 is stratigraphically above section 1 and includes 12 sites covering 110 m of stratigraphic thickness.

[17] Pilot samples from 13 sites had erratic thermal demagnetization behavior and were not further analyzed. From the remaining 13 sites, thermal demagnetization isolated a well-defined ChRM with unblocking temperatures up to 680°C indicating that hematite is the dominant ferrimagnetic mineral (Figure 8b). One site-mean direction with $\alpha_{95} > 25^\circ$ was rejected. Significant dispersion of remaining 12 site-mean directions is observed (Figure 8c and Table 6) and produces an indeterminate result for the reversal test [McFadden and McElhinny, 1990], although normal- and reverse-polarity directions are nearly antipodal. A small increase in between-site grouping of site-mean directions by restoring beds to horizontal is not statistically significant because variation in bedding attitudes is minor. Again the likely primary origin of the ChRM is indicated by the regional field tests reported below.

3.2.5. Two Localities Yielding No Interpretable Results

[18] Twenty-two sites were collected in Paleogene beige-orange fine-grained sandstone to mudstone layers intercalated with conglomerates southeast of Subei (39°24.5'N; 95°24.6'E). Thirteen sites were collected in Neogene flat-lying poorly consolidated buff mudstones in the Yiema Nan Shan (39°15.5'N; 95°44.9'E). For both of these localities, NRM intensity was low, thermal demagnetization of two pilot samples from each site was complete below 300°C, and only a component aligned with the present geomagnetic field was observed. We conclude that these samples contain only a present field secondary magnetization.

3.2.6. Regional Field Tests Within Nan Shan Fold-Thrust Belt

[19] To assess the timing of magnetization with respect to tilting of each of the four sections within the Nan Shan fold thrust belt, a regional fold test was performed (Figure 9). The combined 39 site-mean directions from the four Miocene localities pass a fold test at the 95% significance level and provide a positive reversal test of class C (Figure 9a) [McFadden, 1990; *McFadden and McElhinny*, 1990]. The improved grouping of locality-mean directions in stratigraphic compared with geographic coordinates (Figure 9b)

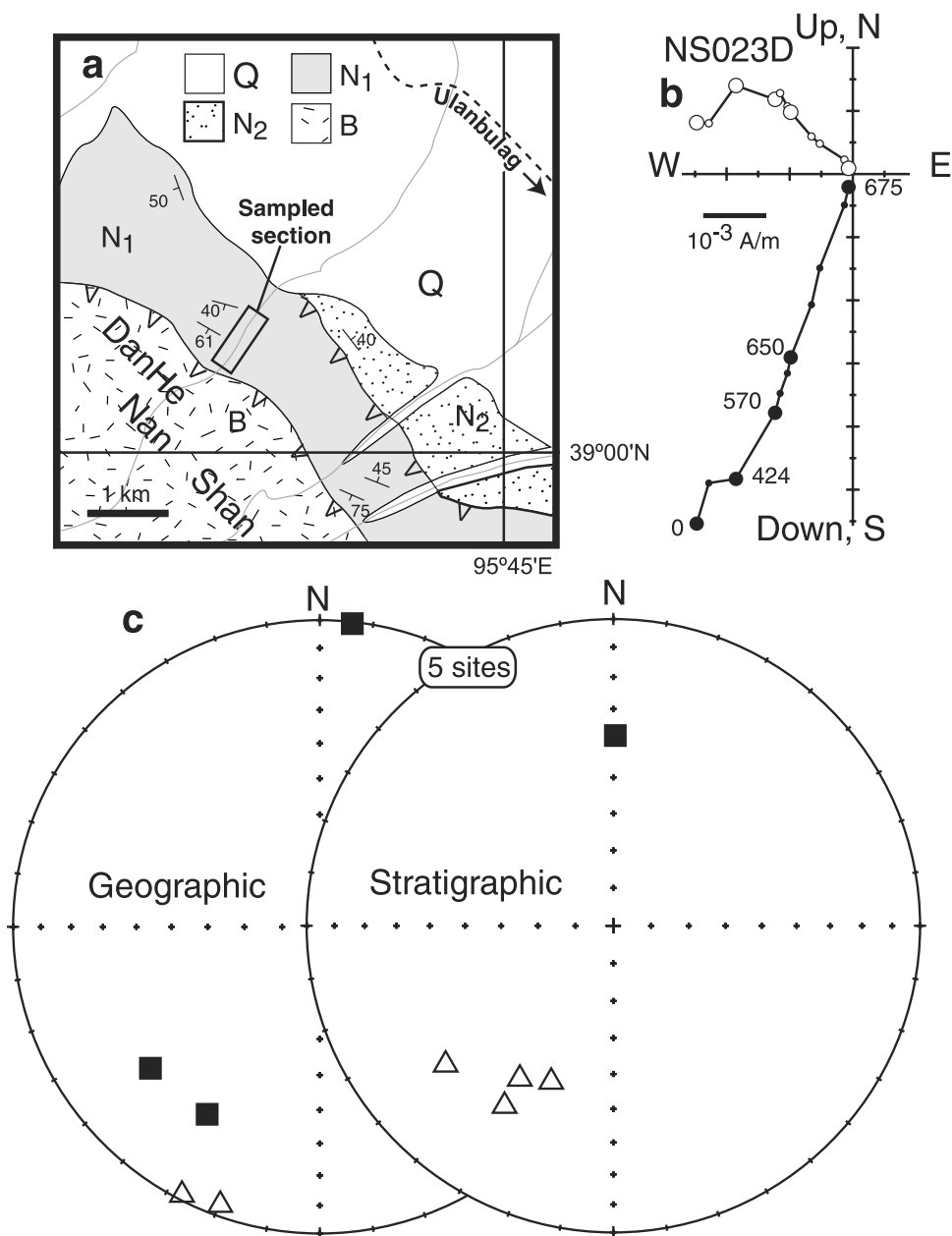


Figure 6. Ulanbulag paleomagnetic locality of the Nan Shan fold-thrust belt. (a) Geologic map in vicinity of sampled section shown by box. (b) Vector endpoint diagram of typical sample in geographic coordinates. (c) Equal-area projection of site-mean ChRM directions in geographic and stratigraphic coordinates. Symbols are as in Figure 4.

Table 4. Site-Mean Directions From the Ulanbulag Paleomagnetic Locality^a

| Sites | Lat °N | Long. °E | Geographic | | Stratigraphic | | α_{95} , deg | <i>k</i> | <i>n/N</i> | Dip, deg | Dip Az, deg |
|--------------------|--------|----------|----------------|----------------|----------------|----------------|---------------------|----------|------------|----------|-------------|
| | | | <i>I</i> , deg | <i>D</i> , deg | <i>I</i> , deg | <i>D</i> , deg | | | | | |
| NS022 | 39.02 | 95.72 | -1.9 | 207.2 | -41.1 | 211.4 | 10.9 | 32.3 | 6/6 | 40.5 | 194.5 |
| NS023 | 39.02 | 95.72 | -4.1 | 199.7 | -44.4 | 201.7 | 16.8 | 11.8 | 7/7 | 40.5 | 194.5 |
| NS024 | 39.02 | 95.72 | 0.7 | 6.1 | 40.1 | 3.2 | 8.5 | 37.9 | 8/8 | 40.0 | 195.5 |
| NS025 ^b | 39.02 | 95.72 | -13.9 | 330.0 | 9.8 | 331.2 | 10.7 | 27.9 | 7/7 | 40.0 | 195.5 |
| NS028 | 39.02 | 95.72 | 29.4 | 211.0 | -31.9 | 211.1 | 7.6 | 47.3 | 8/8 | 61.3 | 211.0 |
| NS029 | 39.02 | 95.72 | 28.8 | 230.1 | -29.7 | 230.3 | 10.1 | 31.4 | 7/7 | 61.3 | 211.0 |
| Mean | 39.02 | 95.72 | -10.5 | 26.1 | | | 22.6 | 12.6 | 5/6 | | |
| Mean | 39.02 | 95.72 | | | 38.5 | 28.3 | 14.4 | 29.3 | 5/6 | | |

^aSee notes for Table 2.

^bSite-mean direction discarded from calculation of the overall locality-mean direction.

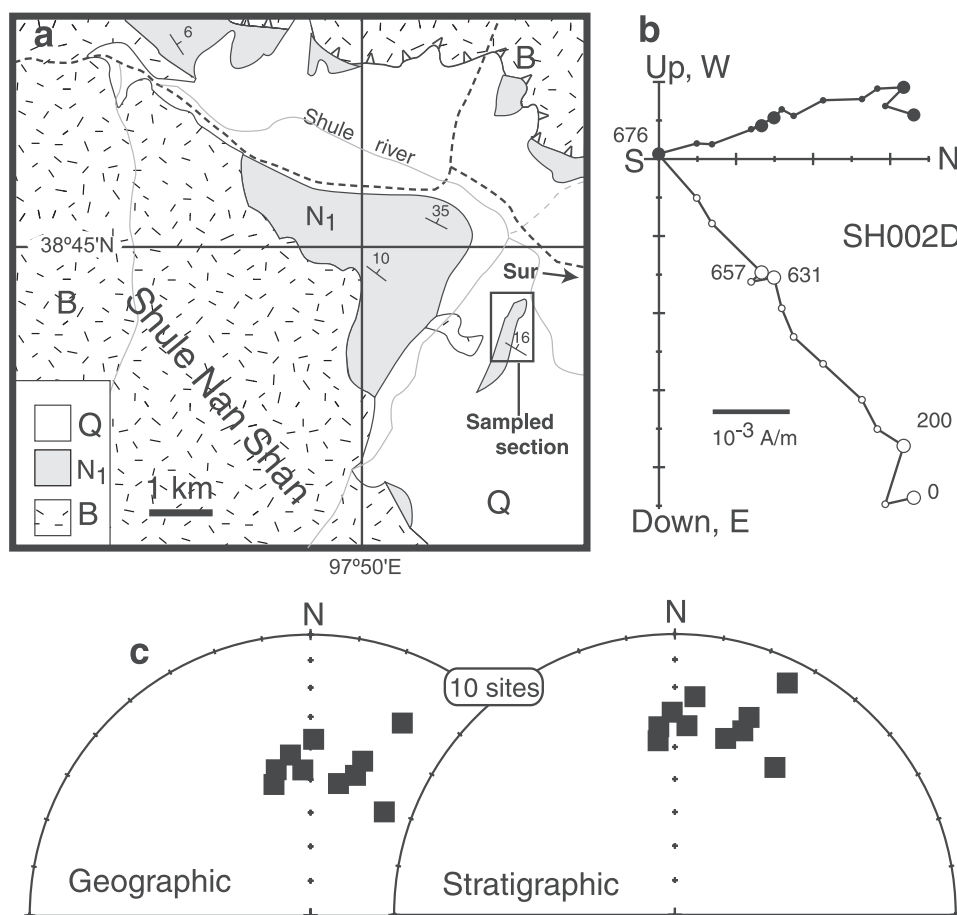


Figure 7. Sur paleomagnetic locality of the Nan Shan fold-thrust belt. (a) Geologic map in vicinity of sampled section shown by box. (b) Vector endpoint diagram of typical sample in geographic coordinates. (c) Equal-area projection of site-mean ChRM directions in geographic and stratigraphic coordinates. Symbols are as in Figure 4.

also provides a positive fold test at 95% significance level [McFadden, 1990] indicating a prefolding magnetization at each of these paleomagnetic localities. The overall mean Miocene paleomagnetic direction for the Nan Shan fold-thrust belt has a concordant declination and a shallow inclination.

3.3. Hexi Corridor

[20] The Hexi corridor lies in the foreland east of the Nan Shan fold-thrust belt (Figure 2). Paleomagnetic samples

were collected from two locations separated by several hundred kilometers within the Hexi corridor.

3.3.1. Yaoquanzi

[21] From this paleomagnetic locality ~10 km northeast of Yumen (Figure 2), 23 sites were collected near the village of Yaoquanzi in brick-red mudstone of the Oligocene Huashaogou (E_{3h}) Formation (Figure 10a, map J-47-II, scale 1:200,000 [Gansu Bureau of Geology and Mineral Resources, 1989]). Sites are distributed over four outcrops covering an estimated 200 m of stratigraphic section with

Table 5. Site-Mean Directions From the Sur Paleomagnetic Locality^a

| Sites | Lat °N | Long °E | Geographic | | Stratigraphic | | α_{95} , deg | k | n/N | Dip, deg | Dip Az, deg |
|-------|--------|---------|------------|-----------|---------------|-----------|---------------------|------|-------|----------|-------------|
| | | | I , deg | D , deg | I , deg | D , deg | | | | | |
| SH001 | 38.73 | 97.97 | 52.7 | 35.5 | 36.7 | 34.1 | 12.5 | 20.6 | 8/8 | 16.0 | 78.0 |
| SH002 | 38.73 | 97.97 | 50.0 | 344.4 | 37.8 | 354.5 | 7.3 | 84.7 | 6/6 | 16.0 | 78.0 |
| SH005 | 38.73 | 97.97 | 37.4 | 1.0 | 23.1 | 5.2 | 14.1 | 19.2 | 7/7 | 16.0 | 78.0 |
| SH006 | 38.73 | 97.97 | 25.1 | 25.5 | 9.1 | 25.9 | 7.1 | 62.3 | 8/8 | 16.0 | 78.0 |
| SH007 | 38.73 | 97.97 | 47.0 | 356.9 | 33.0 | 3.6 | 16.2 | 12.7 | 8/8 | 16.0 | 78.0 |
| SH008 | 38.73 | 97.97 | 45.7 | 346.7 | 33.3 | 355.1 | 17.2 | 13.3 | 7/7 | 16.0 | 78.0 |
| SH009 | 38.73 | 97.97 | 42.0 | 352.9 | 28.7 | 359.2 | 13.8 | 17.1 | 8/8 | 16.0 | 78.0 |
| SH010 | 38.73 | 97.97 | 50.4 | 12.0 | 35.0 | 16.0 | 11.7 | 23.5 | 8/8 | 16.0 | 78.0 |
| SH011 | 38.73 | 97.97 | 46.5 | 17.8 | 30.8 | 20.2 | 7.1 | 61.2 | 8/8 | 16.0 | 78.0 |
| SH012 | 38.73 | 97.97 | 41.6 | 18.7 | 25.9 | 20.6 | 20.0 | 12.2 | 6/6 | 16.0 | 78.0 |
| Mean | 38.73 | 97.97 | 45.0 | 7.3 | 30.0 | 11.6 | 8.8 | 31.3 | 10/10 | | |

^aSee notes for Table 2.

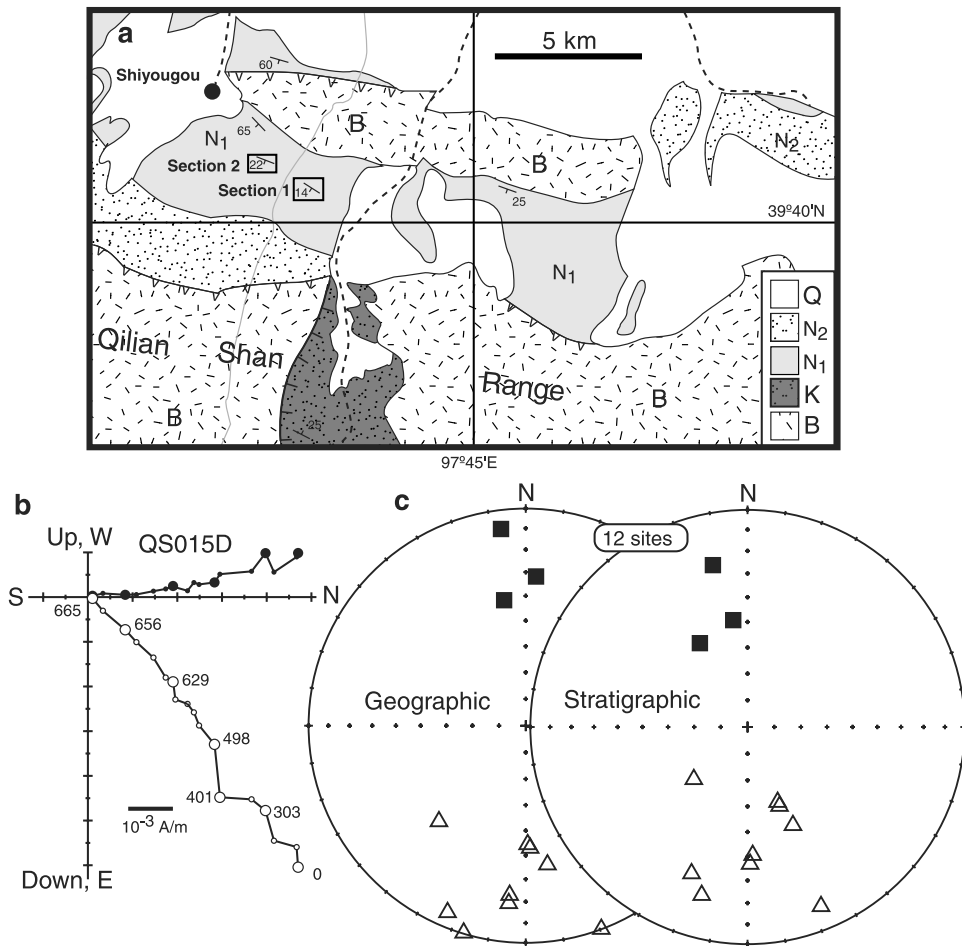


Figure 8. Shiyougou paleomagnetic locality of Nan Shan fold-thrust belt. (a) Geologic map in vicinity of sampled sections shown by boxes. (b) Vector endpoint diagram of typical sample in geographic coordinates. (c) Equal-area projection of site-mean ChRM directions in geographic and stratigraphic coordinates. Symbols are as in Figure 4.

minor variations in bedding attitude. On the basis of thermal demagnetization of two pilot samples from each site, nine sites contain only low intensity NRM that behaves erratically upon demagnetization. From the remaining 14

sites, ChRM was unblocked in the 200°C–600°C temperature range and in the 650°C–690°C range, suggesting a combination of magnetite and hematite (Figure 10b). Two site-mean directions with $\alpha_{95} > 25^\circ$ were discarded. Con-

Table 6. Site-Mean Directions From the Shiyougou Paleomagnetic Locality^a

| Sites | Lat °N | Long °E | Geographic | | Stratigraphic | | α_{95} , deg | <i>k</i> | <i>n/N</i> | Dip, deg | Dip Az, deg |
|------------------|--------|---------|----------------|----------------|----------------|----------------|---------------------|----------|------------|----------|-------------|
| | | | <i>I</i> , deg | <i>D</i> , deg | <i>I</i> , deg | <i>D</i> , deg | | | | | |
| <i>Section 1</i> | | | | | | | | | | | |
| QS005 | 39.68 | 97.67 | -44.5 | 179.1 | -59.4 | 158.2 | 24.9 | 6.8 | 7/7 | 21.7 | 216.4 |
| QS006 | 39.68 | 97.67 | -18.9 | 185.5 | -37.0 | 178.9 | 7.5 | 65.4 | 7/7 | 21.7 | 216.4 |
| QS007 | 39.68 | 97.67 | -0.5 | 196.7 | -20.8 | 195.2 | 10.2 | 30.3 | 8/8 | 21.7 | 216.4 |
| QS008 | 39.68 | 97.67 | 9.6 | 352.8 | 24.8 | 347.9 | 16.5 | 14.3 | 7/7 | 21.7 | 216.4 |
| QS009 | 39.68 | 97.67 | -0.1 | 159.6 | -11.7 | 157.7 | 8.6 | 49.7 | 7/7 | 21.7 | 216.4 |
| QS010 | 39.68 | 97.67 | -43.0 | 177.9 | -57.7 | 158.0 | 10.7 | 75.3 | 4/5 | 21.7 | 216.4 |
| QS012 | 39.68 | 97.67 | -7.5 | 202.7 | -28.6 | 200.9 | 20.6 | 14.7 | 5/5 | 21.7 | 216.4 |
| <i>Section 2</i> | | | | | | | | | | | |
| QS015 | 39.70 | 97.65 | 31.7 | 3.9 | 45.2 | 1.0 | 5.5 | 151.9 | 6/6 | 14.0 | 197.3 |
| QS016 | 39.70 | 97.65 | 41.0 | 350.2 | 53.0 | 342.4 | 13.6 | 32.6 | 5/5 | 14.0 | 197.3 |
| QS019 | 39.70 | 97.65 | -40.2 | 222.2 | -52.6 | 229.2 | 13.4 | 21.3 | 7/7 | 14.0 | 197.3 |
| QS021 | 39.70 | 97.65 | -22.7 | 185.4 | -36.4 | 183.6 | 21.0 | 9.2 | 7/7 | 14.0 | 197.3 |
| QS022 | 39.70 | 97.65 | -35.5 | 171.2 | -47.8 | 165.1 | 11.1 | 69.2 | 4/5 | 14.0 | 197.3 |
| Mean | 39.69 | 97.66 | 25.5 | 3.7 | | | 12.3 | 13.2 | 12/12 | | |
| Mean | 39.69 | 97.66 | | | 41.3 | 358.4 | 12.4 | 13.8 | 12/12 | | |

^aSee notes for Table 2.

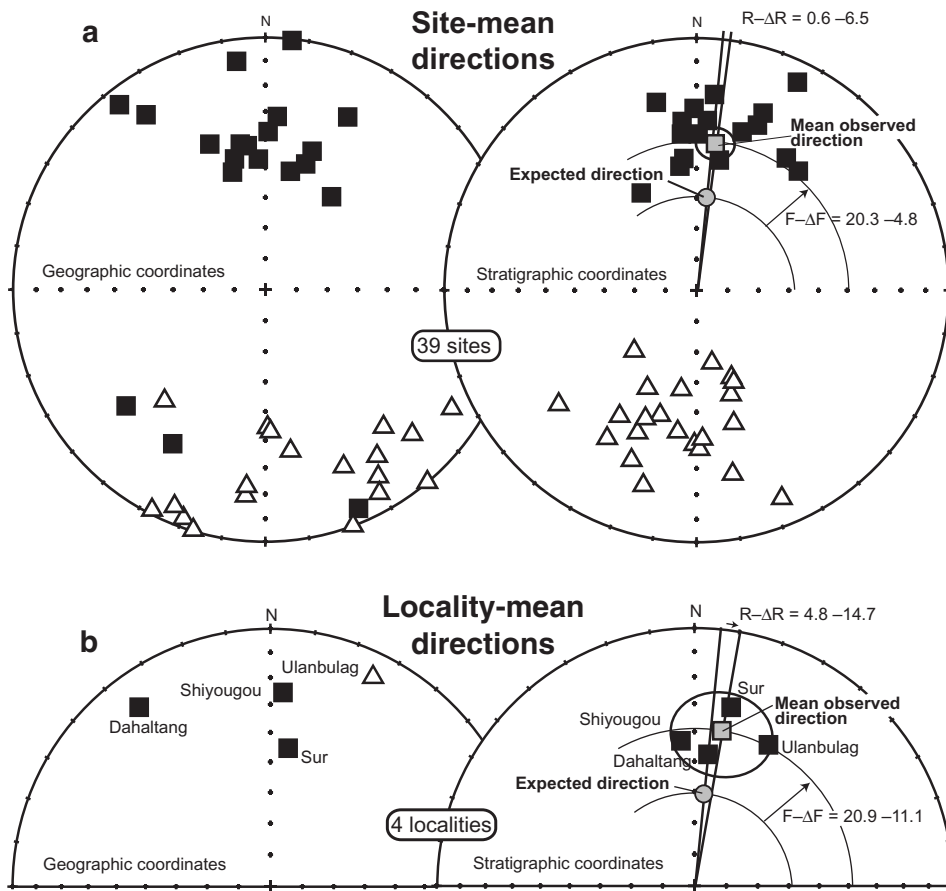


Figure 9. Equal-area projections of site-mean and locality-mean ChRM directions from four localities across the Nan Shan fold-thrust belt. In stratigraphic coordinates, the gray square is overall mean observed direction with surrounding 95% confidence limit. Gray circle is the expected direction calculated from the Miocene paleomagnetic pole of Eurasia. Vertical axis rotation ($R \pm \Delta R$) and inclination flattening ($F \pm \Delta F$) are calculated from comparison of observed and expected directions (Table 1).

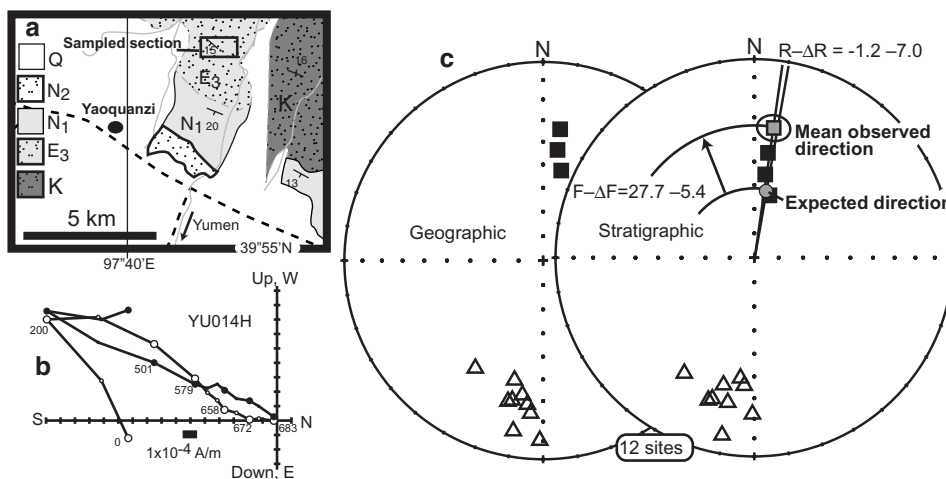


Figure 10. Yaoquanzi paleomagnetic locality of Hexi Corridor. (a) Geologic map in vicinity of sampled section shown by box. (b) Vector endpoint diagram of typical sample in geographic coordinates. (c) Equal-area projection of site-mean ChRM directions in geographic and stratigraphic coordinates. Symbols are as in Figure 4. Gray circle is the expected direction calculated from the Oligocene paleomagnetic pole of Eurasia.

Table 7. Site-Mean Directions From the Yaoquanzi Paleomagnetic Locality^a

| Sites | Lat °N | Long °E | Geographic | | Stratigraphic | | α_{95} , deg | k | n/N | Dip, deg | Dip Az, deg |
|-------|--------|---------|------------|-----------|---------------|-----------|---------------------|-------|-------|----------|-------------|
| | | | I , deg | D , deg | I , deg | D , deg | | | | | |
| YU005 | 39.97 | 97.68 | -27.8 | 194.0 | -34.9 | 191.8 | 16.2 | 12.6 | 8/8 | 8.0 | 220.0 |
| YU007 | 39.97 | 97.68 | -28.8 | 192.5 | -35.8 | 190.0 | 14.1 | 19.2 | 7/7 | 8.0 | 220.0 |
| YU008 | 39.97 | 97.68 | -28.0 | 186.3 | -34.5 | 183.5 | 15.9 | 15.4 | 7/7 | 8.0 | 220.0 |
| YU011 | 39.97 | 97.68 | -32.1 | 188.7 | -38.9 | 186.5 | 10.6 | 33.1 | 7/7 | 7.5 | 212.0 |
| YU014 | 39.97 | 97.68 | -36.2 | 212.2 | -44.1 | 211.2 | 18.9 | 8.4 | 9/9 | 8.0 | 220.0 |
| YU015 | 39.97 | 97.68 | -38.1 | 193.4 | -45.1 | 190.0 | 7.8 | 60.5 | 7/7 | 8.0 | 220.0 |
| YU016 | 39.97 | 97.68 | -14.0 | 190.0 | -20.7 | 188.7 | 15.2 | 14.3 | 8/8 | 8.0 | 220.0 |
| YU017 | 39.97 | 97.68 | -23.9 | 184.6 | -30.3 | 182.2 | 11.6 | 23.8 | 8/8 | 8.0 | 220.0 |
| YU018 | 39.97 | 97.68 | -10.4 | 181.1 | -16.6 | 179.8 | 12.2 | 31.0 | 6/6 | 8.0 | 220.0 |
| YU019 | 39.97 | 97.68 | 51.6 | 11.8 | 39.7 | 10.9 | 12.1 | 31.4 | 6/6 | 12.0 | 7.0 |
| YU020 | 39.97 | 97.68 | 33.8 | 7.4 | 21.8 | 7.3 | 4.0 | 232.9 | 7/7 | 12.0 | 7.0 |
| YU021 | 39.97 | 97.68 | 43.2 | 7.4 | 31.2 | 7.4 | 21.7 | 13.4 | 4/5 | 12.0 | 7.0 |
| Mean | 39.97 | 97.68 | 30.9 | 10.5 | | | 7.1 | 37.8 | 12/12 | | |
| Mean | 39.97 | 97.68 | | | 33.0 | 8.6 | 6.0 | 53.7 | 12/12 | | |

^aSee notes for Table 2.

sistent with a primary origin for the ChRM, the remaining 12 site-mean directions (Table 7 and Figure 10c) pass the fold test at 95% confidence level [McFadden, 1990] and a reversals test of class C [McFadden and McElhinny, 1990]. The mean direction yields no significant rotation and shallowed inclinations when compared to the expected direction calculated using the Oligocene paleomagnetic pole for Eurasia (Figure 10c).

3.3.2. Longshou Shan

[22] Paleomagnetic samples were collected from two sections within the Longshou range north of Zhangye (Figures 2 and 11a). Each section was ~100 m thick and a total of 38 sites were collected from subhorizontal purple to brown well-indurated siltstones of the Early Cretaceous Upper Miaogou Group (K₁mg^b, map J-47-XI, scale 1:200,000 [Gansu Bureau of Geology and Mineral Resources, 1989; Wang and Coward, 1993]). The sampled strata are within the 2.5-km-thick Renzongkou section described by Vincent and Allen [1999]. They assigned an Aptian-Albian age based on occurrence of *Stellatochara mundula*.

[23] For most sites, thermal demagnetization revealed a well-defined univectorial ChRM unblocked between 500°C and 680°C (Figure 11b). Erratic directions were observed in samples from two sites that were discarded from further analysis. Within-site dispersion of the remaining 36 site-mean directions is small as expressed by high k values (Table 8). This dispersion is less than anticipated for random time sampling of the ancient geomagnetic field. We interpret the low dispersion to result from time integration of the geomagnetic field over 100–1000 year time intervals during postdepositional oxidation and acquisition of the ChRM as a chemical remanent magnetization (CRM). Variations in bedding attitude are insufficient to provide a definitive fold test and all directions are normal polarity as expected for rocks deposited during the Cretaceous Normal-Polarity Superchron. The overall observed mean direction is concordant with the expected Aptian-Albian direction at the Longshou Shan locality (Figure 11c).

4. Discussion and Conclusions

4.1. Hexi Corridor

[24] On the basis of paleomagnetic results from Cretaceous red beds in the Qilian Shan thrust front, Frost *et al.*

[1995] concluded that the Hexi corridor had rotated ~30° clockwise (result 7 in Table 1 and Figure 2). However, the paleomagnetic directions reported here from Early Cretaceous rocks of the Longshou Shan and from Oligocene rocks at Yaoquanzi have concordant declinations when compared with expected declinations calculated from equivalent age Eurasian reference poles. In addition, concordant paleomagnetic directions were recently reported from Early Cretaceous red beds near Yumen [Chen *et al.*, 2002b]. The available paleomagnetic data thus indicate that, in terms of tectonic rotations, the Hexi corridor has been a stable part of the Eurasian plate since at least Early Cretaceous time. The discordant declination observed by Frost *et al.* [1995] is likely the result of a local rotation related to the Qilian thrust and we list those results along with others from the Nan Shan fold-thrust belt.

[25] On a more regional scale, concordant paleomagnetic directions are observed in Early Cretaceous rocks of the Ordos Basin [Sun *et al.*, 2001] and in the North China blocks [Ma *et al.*, 1993; Chen *et al.*, 2002b]. Early Cretaceous paleomagnetic directions from the Tarim Basin are concordant with results from the Hexi corridor [see Dupont-Nivet *et al.*, 2002b] and paleomagnetic results from Tertiary red beds in the Qaidam Basin indicate no vertical axis rotation since Oligocene time [Dupont-Nivet *et al.*, 2002a]. South of the Hexi corridor along the eastern fringe of the Tibetan Plateau, clockwise vertical axis rotations of Early Cretaceous paleomagnetic directions are reported in the Xining-Lanzhou area [Halim *et al.*, 1998; Yang *et al.*, 2002] and are widespread within eastern Tibet [Lin and Watts, 1988; Otofujii *et al.*, 1990; Huang *et al.*, 1992].

[26] The regional pattern of paleomagnetic data indicate: (1) the Hexi corridor has been (in terms of tectonic rotations) a stable part of the North China block since Early Cretaceous time; and (2) widespread clockwise vertical axis rotations have affected the eastern fringe of the Tibetan Plateau but do not extend north into the Hexi corridor. This pattern suggests the presence of an important post-Early Cretaceous tectonic boundary separating the Hexi corridor from eastern Tibet.

4.2. Nan Shan Fold-Thrust Belt and Qaidam Basin

[27] The overall mean paleomagnetic direction from 39 sites of our 4 sampling localities across the Nan Shan fold-thrust belt has a concordant declination and shallow incli-

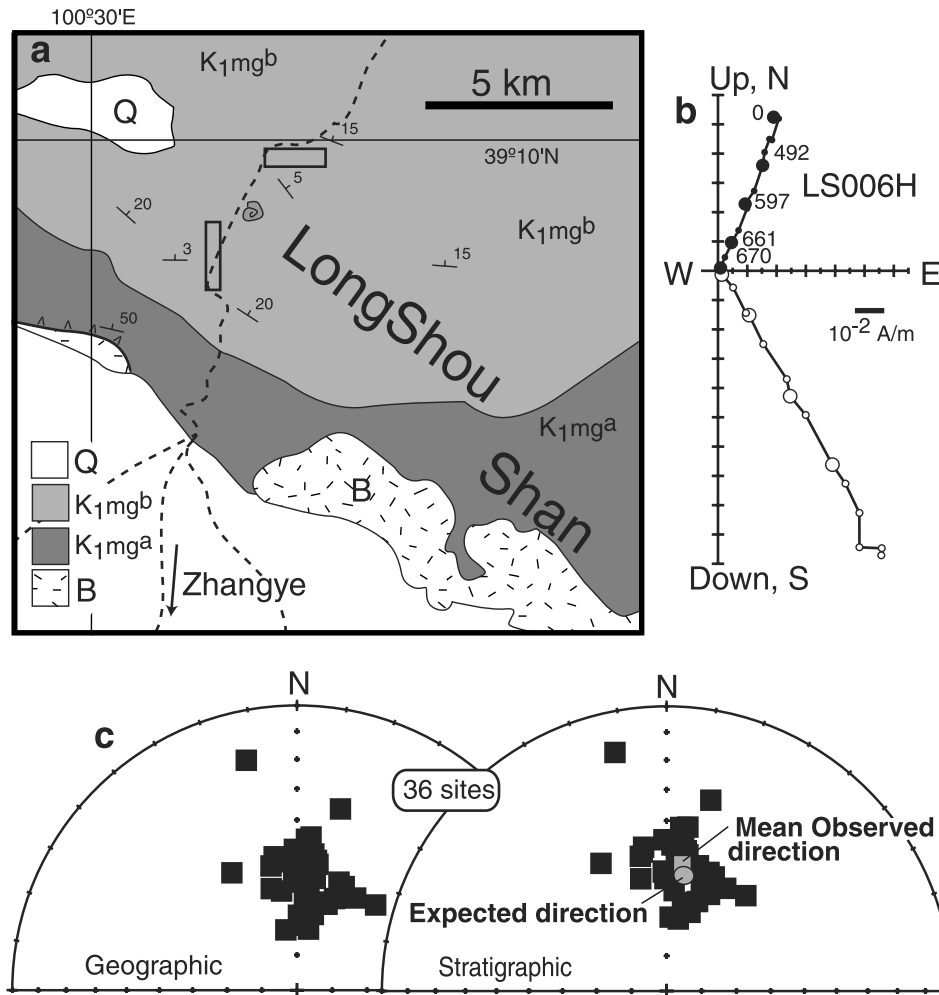


Figure 11. LongShou paleomagnetic locality of Hexi Corridor. (a) Geologic map in vicinity of sampled sections shown by boxes. K_1mg^a and K_1mg^b are Early Cretaceous Lower and Upper Miaogou group, respectively. Other map patterns are as in Figure 4. (b) Vector endpoint diagram of typical sample in geographic coordinates. (c) Equal-area projection of site-mean ChRM directions in geographic and stratigraphic coordinates. Symbols are as in Figure 4. Gray circle is the expected direction calculated from the Early Cretaceous paleomagnetic pole of Eurasia.

nation (Figures 9a and 9b and Table 1). Inspection of results from individual localities suggests that small local rotations may have affected some sampled sections but these are neither statistically significant nor systematic. The concordant mean declination indicates no significant rotation of the Nan Shan fold-thrust belt since Miocene time. Previous paleomagnetic results from the Nan Shan fold-thrust belt also indicated the possibility of some local rotations but no significant overall rotation of the fold-thrust belt (Table 1). These results support the conclusion of Meyer *et al.* [1998] that differential shortening with attendant clockwise rotation of the Nan Shan fold-thrust belt is not a significant tectonic process within northeastern Tibet during Neogene time. Instead, Neogene compressional deformation within the Nan Shan fold-thrust belt has occurred without vertical axis rotation.

[28] The absence of Neogene rotation of the Nan Shan fold-thrust belt suggests that the adjacent Qaidam Basin has translated without vertical axis rotation toward the northeast by strike-slip motion on the Altyn Tagh fault. Dupont-Nivet

et al. [2002a] reported paleomagnetic data that directly constrain Neogene vertical axis rotation of the Qaidam Basin. Concordant paleomagnetic declinations were obtained from red sedimentary rocks of the Oligocene Gancaigou Formation at two locations separated by several hundred kilometers: 55 km south of the Altyn Tagh fault at E Bo Liang ($R \pm \Delta R = -1.7^\circ \pm 6.8^\circ$, Table 1 and Figure 2) and within a broad anticline 20 km west of Xiaoqaidam ($R \pm \Delta R = 1.5^\circ \pm 12.2^\circ$, Table 1 and Figure 2). These paleomagnetic data from Oligocene rocks within the central basin clearly indicate that no Neogene vertical axis tectonic rotation exceeding 10° has affected the Qaidam Basin. However, Chen *et al.* [2002a] have argued that paleomagnetic observations from three localities indicate a post-Oligocene $\sim 20^\circ$ clockwise rotation of the Qaidam Basin [Chen *et al.*, 2002a, Figure 5]. We disagree with this interpretation on several grounds.

[29] Chen *et al.* [2002a] use paleomagnetic data from Early Cretaceous rocks located near Lanzhou (Figure 2) to infer clockwise rotation of the Qaidam Basin. However,

Table 8. Site-Mean Directions From the Longshou Paleomagnetic Locality^a

| Sites | Lat (°N) | Long (°E) | Geographic | | Stratigraphic | | α_{95} , deg | k | n/N | Dip, deg | Dip Az, deg |
|-------|----------|-----------|------------|-----------|---------------|-----------|---------------------|-------|-------|----------|-------------|
| | | | I , deg | D , deg | I , deg | D , deg | | | | | |
| LS001 | 39.05 | 100.45 | 50.8 | 350.3 | 47.6 | 350.9 | 4.5 | 224.5 | 6/6 | 3.2 | 0.0 |
| LS002 | 39.05 | 100.45 | 51.1 | 331.0 | 48.3 | 332.7 | 5.4 | 126.7 | 7/7 | 3.2 | 0.0 |
| LS003 | 39.05 | 100.45 | 56.6 | 42.8 | 54.2 | 39.7 | 3.0 | 345.5 | 8/8 | 3.2 | 0.0 |
| LS004 | 39.05 | 100.45 | 50.2 | 7.0 | 47.0 | 6.6 | 5.8 | 91.1 | 8/8 | 3.2 | 0.0 |
| LS005 | 39.05 | 100.45 | 72.3 | 10.7 | 69.1 | 9.1 | 4.8 | 157.0 | 7/7 | 3.2 | 0.0 |
| LS006 | 39.05 | 100.45 | 58.6 | 32.5 | 55.8 | 29.9 | 8.4 | 53.1 | 7/7 | 3.2 | 0.0 |
| LS007 | 39.05 | 100.45 | 59.9 | 345.8 | 56.8 | 347.0 | 10.4 | 55.1 | 5/5 | 3.2 | 0.0 |
| LS008 | 39.05 | 100.45 | 51.6 | 5.7 | 48.4 | 5.3 | 7.9 | 72.6 | 6/6 | 3.2 | 0.0 |
| LS009 | 39.05 | 100.45 | 50.7 | 2.2 | 47.5 | 2.1 | 5.3 | 159.5 | 6/6 | 3.2 | 0.0 |
| LS010 | 39.05 | 100.45 | 53.1 | 9.5 | 49.9 | 8.9 | 8.8 | 40.2 | 8/8 | 3.2 | 0.0 |
| LS011 | 39.05 | 100.45 | 64.3 | 4.7 | 61.1 | 4.3 | 3.7 | 325.6 | 6/6 | 3.2 | 0.0 |
| LS012 | 39.05 | 100.45 | 61.6 | 22.3 | 58.6 | 20.3 | 6.8 | 66.8 | 8/8 | 3.2 | 0.0 |
| LS013 | 39.05 | 100.45 | 45.1 | 5.2 | 41.9 | 5.0 | 7.2 | 60.3 | 8/8 | 3.2 | 0.0 |
| LS014 | 39.05 | 100.45 | 18.5 | 347.6 | 15.4 | 347.8 | 5.4 | 107.1 | 8/8 | 3.2 | 0.0 |
| LS015 | 39.05 | 100.45 | 34.9 | 13.5 | 31.8 | 13.0 | 5.5 | 100.6 | 8/8 | 3.2 | 0.0 |
| LS016 | 39.05 | 100.45 | 58.8 | 358.3 | 55.6 | 358.4 | 6.7 | 83.1 | 7/7 | 3.2 | 0.0 |
| LS017 | 39.05 | 100.45 | 53.3 | 348.2 | 50.2 | 349.0 | 3.7 | 262.1 | 7/7 | 3.2 | 0.0 |
| LS018 | 39.05 | 100.45 | 49.1 | 359.0 | 45.9 | 359.0 | 3.8 | 214.5 | 8/8 | 3.2 | 0.0 |
| LS019 | 39.05 | 100.45 | 52.8 | 357.6 | 49.6 | 357.8 | 3.4 | 260.1 | 8/8 | 3.2 | 0.0 |
| LS020 | 39.05 | 100.45 | 54.6 | 4.5 | 51.4 | 4.2 | 2.7 | 502.6 | 7/7 | 3.2 | 0.0 |
| LS021 | 39.05 | 100.45 | 52.0 | 8.5 | 48.8 | 8.0 | 9.2 | 43.9 | 7/7 | 3.2 | 0.0 |
| LS022 | 39.05 | 100.45 | 57.2 | 24.5 | 54.3 | 22.7 | 8.6 | 42.4 | 8/8 | 3.2 | 0.0 |
| LS023 | 39.05 | 100.45 | 56.6 | 21.2 | 53.6 | 19.6 | 8.6 | 42.5 | 8/8 | 3.2 | 0.0 |
| LS024 | 39.12 | 100.55 | 56.1 | 359.9 | 52.8 | 5.2 | 8.9 | 57.1 | 6/6 | 5.0 | 51.6 |
| LS027 | 39.12 | 100.55 | 63.9 | 19.3 | 59.6 | 23.9 | 6.2 | 152.2 | 5/5 | 5.0 | 51.6 |
| LS028 | 39.17 | 100.58 | 57.3 | 9.3 | 52.6 | 14.2 | 10.5 | 77.3 | 4/4 | 5.9 | 47.9 |
| LS029 | 39.17 | 100.58 | 64.4 | 13.2 | 59.4 | 19.1 | 4.5 | 149.4 | 8/8 | 5.9 | 47.9 |
| LS030 | 39.17 | 100.58 | 63.9 | 14.2 | 58.9 | 19.8 | 8.7 | 48.8 | 7/7 | 5.9 | 47.9 |
| LS031 | 39.17 | 100.58 | 67.8 | 12.2 | 62.8 | 19.0 | 5.3 | 301.8 | 4/4 | 5.9 | 47.9 |
| LS032 | 39.17 | 100.58 | 59.1 | 6.4 | 54.5 | 12.0 | 11.7 | 23.3 | 8/8 | 5.9 | 47.9 |
| LS033 | 39.17 | 100.58 | 56.8 | 1.2 | 52.6 | 7.0 | 11.5 | 34.9 | 6/6 | 5.9 | 47.9 |
| LS034 | 39.17 | 100.58 | 71.3 | 7.6 | 66.5 | 16.5 | 5.9 | 107.1 | 7/7 | 5.9 | 47.9 |
| LS035 | 39.17 | 100.58 | 72.5 | 349.5 | 68.8 | 2.7 | 9.0 | 74.0 | 5/5 | 5.9 | 47.9 |
| LS036 | 39.17 | 100.58 | 68.6 | 1.1 | 64.2 | 10.2 | 4.6 | 215.1 | 6/6 | 5.9 | 47.9 |
| LS037 | 39.17 | 100.58 | 45.9 | 3.6 | 41.6 | 7.4 | 9.8 | 33.0 | 8/8 | 5.9 | 47.9 |
| LS038 | 39.17 | 100.58 | 61.2 | 351.2 | 57.6 | 359.1 | 8.8 | 40.2 | 8/8 | 5.9 | 47.9 |
| Mean | 39.09 | 100.50 | 57.0 | 4.9 | | | 3.8 | 40.4 | 36/36 | | |
| Mean | 39.09 | 100.50 | | | 53.4 | 6.8 | 3.8 | 40.5 | 36/36 | | |

^aSee notes for Table 2.

many Cenozoic structures separate the Qaidam Basin from Lanzhou so these areas have not behaved as a single rigid crustal block during Cenozoic development of the Tibetan Plateau. *Chen et al.* [2002a] also report clockwise rotations of paleomagnetic declinations from Late Jurassic strata north of the Qaidam Basin near Huatugou (Figure 2). At the same locality, paleomagnetic directions from Early Cretaceous strata unconformably overlying the Late Jurassic strata [see *Chen et al.*, 2002a, p. 6–3–[6] and Table 1, p. 6–4] indicate a smaller (insignificant?) clockwise rotation of $8.1^\circ \pm 7.1^\circ$ (Figure 2 and Table 1). Although not interpreted as such by *Chen et al.* [2002a] the Early Cretaceous results suggest that most of the rotation recorded in the Late Jurassic rocks at Huatugou occurred between Late Jurassic and Early Cretaceous times rather than during the Neogene.

[30] Finally, *Chen et al.* [2002a] use paleomagnetic results from a locality near Mahai to support Neogene clockwise rotation of the Qaidam Basin. This locality is within the southern Nan Shan fold-thrust belt structurally allochthonous to the basin (Figure 2, map J-46-XVII [*Qinghai Bureau of Geology and Mineral Resources*, 1991]). Mapping of geologic structures in this area indicates that the Mahai rocks are within imbricated thrust sheets at the northwestern termina-

tion of a southwest vergent thrust salient [*Robinson et al.*, 2002a]. Emplacement of this thrust salient with decreasing shortening toward the northwest termination is consistent with local clockwise rotation of the Mahai locality. Thus the rotation indicated by the paleomagnetic results from the Mahai locality is likely a local rotation rather than an indication of rotation of the adjacent Qaidam Basin. In addition, *Chen et al.* [2002a] could not distinguish whether the samples collected near Mahai were from the Paleocene-Eocene Luhele Formation or from the Oligocene Gancaigou Formation [see *Chen et al.*, 2002a, p. 6–6–[9]]. So even if the sampled rocks have not been affected by a local rotation and these data do indicate vertical axis rotation of the Qaidam Basin, the Mahai strata may belong to the Paleocene-Eocene Luhele Formation with the implication that clockwise rotation of the basin occurred before deposition of the Oligocene Gancaigou Formation. In either case, rotation of the Mahai rocks cannot be taken to indicate Neogene rotation of the Qaidam Basin.

[31] With net Neogene rotation of the Qaidam Basin limited to $<10^\circ$, the time-integrated rate of vertical axis tectonic rotation must be less than $0.4^\circ/\text{m.y.}$ This low rate of rotation favors kinematic models that imply little or no

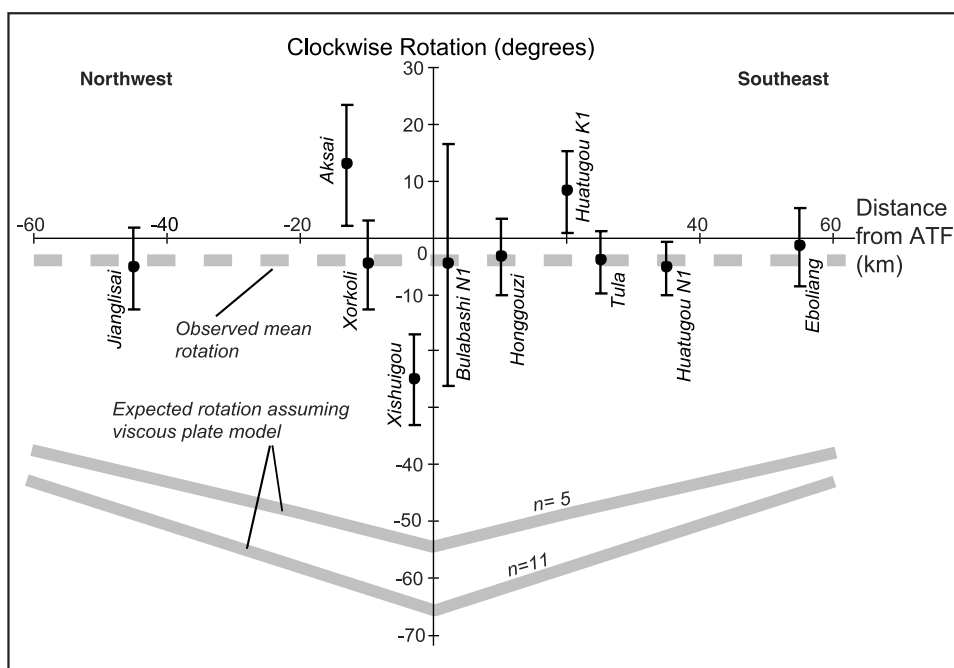


Figure 12. Clockwise Cenozoic vertical axis rotations plotted against approximate distance from the Altyn Tagh fault. Dashed gray line indicates the mean observed rotation. Solid gray lines are expected rotations calculated assuming transcurrent deformation of thin viscous sheet with stress exponent $n = 5$ and $n = 11$ (see Appendix A).

Neogene rotation of the Qaidam Basin [England and Molnar, 1997; Holt and Haines, 1993; Holt et al., 2000] over models that predict larger rotations [Avouac and Tapponnier, 1993; Peltzer and Saucier, 1996].

4.3. Altyn Tagh Range and Concentration of Shear on the Altyn Tagh Fault

[32] When compared to the expected Oligocene direction, the observed paleomagnetic directions from the Xorkoli Valley indicate no significant rotation ($R \pm \Delta R = -4.8^\circ \pm 7.7^\circ$). Similar results are reported from Neogene red beds at three other localities within the Altyn Tagh range (Table 1). We note that, although barely resolvable at the 95% precision level, these paleomagnetic results are consistent with the 5° counterclockwise rotation predicted by a strike-slip duplex structural model for the Altyn Tagh range [Cowgill et al., 2000]. However, the first-order result is small or no significant Neogene rotation ($<10^\circ$) for the Altyn Tagh range and limited Neogene rotation ($<10^\circ$) of the Qaidam and Tarim basins [Dupont-Nivet et al., 2002a, 2002b]. In turn, limited Neogene rotations north and south of the fault imply that the ATF has not rotated significantly since 25 Ma.

[33] Compilation of the growing paleomagnetic data available from the vicinity of the ATF provides additional constraints for Tertiary regional tectonics. Vertical axis rotations indicated by paleomagnetic results from localities within 60 km of the ATF (Figure 2) are illustrated in Figure 12. The average vertical axis rotation is -3.4° (gray dashed line on Figure 12). For reference, the expected counterclockwise vertical axis rotation of rigid blocks floating on a continuum deforming according to a thin viscous plate model in a sinistral shear system is also

plotted on Figure 12 [England et al., 1985; Sonder et al., 1986; Nelson and Jones, 1987] (see Appendix A). The absence of significant rotations in the vicinity of the ATF fault indicates that shear is not distributed across a wide area but rather is concentrated on the fault. A similar conclusion resulted from detailed paleomagnetic and structural analysis of the arcuate Tula syncline indicating that the curvature of this structure is a primary expression of thrusting over an arcuate ramp rather than shear distributed south of the fault [Dupont-Nivet et al., 2003]. The lack of distributed shear implies that strike-slip offset of geological piercing points measured directly on the fault trace provide accurate determinations of displacement [Yin and Harrison, 2000; Yue et al., 2001]. Furthermore, localized shear implies that the ATF is weak relative to the strength of the surrounding blocks. This supports that the ATF is of lithospheric scale [Wittlinger et al., 1998], a necessary condition for extrusion tectonics [Tapponnier et al., 1982, 1986]. However, limited ATF offset transferring motion from one belt of crustal thickening to another [Burchfiel et al., 1989] without vertical axis rotation of northern Tibet precludes extrusion as the dominant tectonic mechanism during Neogene time. Instead, a combination of distributed deformation and thickening of the lithosphere with concentration of shear along narrow strike-slip zones has been proposed by Holt et al. [2000] (Figure 1b). This model has considerable merit for explaining the overall pattern of vertical axis rotations indicated by the paleomagnetic data from northern Tibet.

Appendix A

[34] Vertical axis rotations experienced by rigid blocks floating on a deforming thin viscous plate along a trans-

current fault have been modeled by England *et al.* [1985], Nelson and Jones [1987], and Sonder and England [1986]. Near the center of the modeled transcurrent fault, vertical axis rotation of rigid blocks is given by

$$\theta = \tan^{-1} [(2D\pi\sqrt{n/\lambda}) \exp(-4y\pi\sqrt{n/\lambda})],$$

where θ is the angle of vertical axis rotation, y is the distance from the fault, $\lambda/2$ is the length of the fault (chosen as 1500 km for the ATF), n is the stress exponent (chosen between 5 and 11 for Tibet) [Sonder and England, 1986], and D is the fault displacement (chosen as 300 km for the ATF).

[35] **Acknowledgments.** This work was funded by grant EAR 9725663 from the Continental Dynamics Program of the National Science Foundation. We thank Wang Xiao-Feng at the Institute of Geomechanics, Chinese Academy of Geological Sciences, for providing logistical support, Lucas Murray and Bill Hart for laboratory assistance, George Gehrels for help in the field, Guo Zhaojie for assistance with the Chinese literature, Alex Robinson for sharing his unpublished mapping of the northeastern Qaidam Basin, and Robert Fromm for extensive discussions. Part of the paleomagnetic analysis was performed using software by R. J. Enkin. We are grateful to J. W. Geissmann, P. R. Cobbold, and R. J. Enkin for constructive and detailed reviews.

References

- Argand, E., La tectonique de l'Asie, *Int. Geol. Cong. Rep. Session, 13*, 170–372, 1924.
- Avouac, J. P., and P. Tapponnier, Kinematic model of active deformation in central Asia, *Geophys. Res. Lett.*, *20*(10), 895–898, 1993.
- Beck, M. E., Paleomagnetic record of plate-margin tectonic processes along the western edge of North America, *J. Geophys. Res.*, *85*(B12), 7115–7131, 1980.
- Bendick, R., R. Bilham, J. Freymueller, K. Larson, and G. Yin, Geodetic evidence for a low slip rate in the Altyn Tagh fault system, *Nature*, *404*(6773), 69–72, 2000.
- Besse, J., and V. Courtillot, Paleogeographic maps of the continents bordering the Indian Ocean since the Early Jurassic, *J. Geophys. Res.*, *93*(B10), 11,791–11,808, 1988.
- Besse, J., and V. Courtillot, Apparent and true polar wander and the geometry of the geomagnetic field over the last 200 Myr, *J. Geophys. Res.*, *107*(B11), 2300, doi:10.1029/2000JB000050, 2002.
- Burchfiel, B. C., D. Quidong, P. Molnar, L. Royden, W. Yipeng, Z. Peizhen, and Z. Weiqi, Intra-crustal detachment zones of continental deformation, *Geology*, *17*(8), 448–452, 1989.
- Butler, R. F., *Paleomagnetism: Magnetic Domains to Geologic Terranes*, pp. 83–104, Blackwell Sci., Malden, Mass., 1992.
- Chen, Y., S. Gilder, N. Halim, J.-P. Cogné, and V. Courtillot, New paleomagnetic constraints on central Asian kinematics: Displacement along the Altyn Tagh fault and rotation of the Qaidam Basin, *Tectonics*, *21*(5), 1042, doi:10.1029/2001TC901030, 2002a.
- Chen, Y., H. Wu, V. Courtillot, and S. Gilder, Large N-S convergence at the northern edge of the Tibetan Plateau? New Early Cretaceous paleomagnetic data from the Hexi Corridor, NW China, *Earth Planet. Sci. Lett.*, *201*, 293–307, 2002b.
- Chen, Z., B. C. Burchfiel, Y. Liu, R. W. King, L. H. Royden, W. Tang, E. Wang, J. Zhao, and X. Zhang, Global Positioning System measurements from eastern Tibet and their implications for India/Eurasia intercontinental deformation, *J. Geophys. Res.*, *105*(B7), 16,215–16,227, 2000.
- Cobbold, P. R., and P. Davy, Indentation tectonics in nature and experiments, 2. Central Asia, *Bull. Geol. Ins. Uppsala*, *14*, 143–162, 1988.
- Cowgill, E., A. Yin, W. X. Feng, and Z. Qing, Is the North Altyn fault part of a strike-slip duplex along the Altyn Tagh fault system?, *Geology*, *28*(3), 255–258, 2000.
- Demarest, H. H., Error analysis of the determination of tectonic rotations from paleomagnetic data, *J. Geophys. Res.*, *88*, 4321–4328, 1983.
- Dupont-Nivet, G., R. F. Butler, A. Yin, and X. Chen, Paleomagnetism indicates no Neogene rotation of the Qaidam Basin in North Tibet during Indo-Asian Collision, *Geology*, *30*(3), 263–266, 2002a.
- Dupont-Nivet, G., Z. Guo, R. F. Butler, and C. Jia, Discordant paleomagnetic direction in Miocene rocks from the central Tarim Basin: Evidence for local deformation and inclination shallowing, *Earth Planet. Sci. Lett.*, *199*, 473–482, 2002b.
- Dupont-Nivet, G., R. F. Butler, A. Yin, D. Robinson, Y. Zhang, W. S. Qiao, and J. Melosh, Concentration of crustal displacement along a weak Altyn Tagh fault: Evidence from paleomagnetism of the northern Tibetan Plateau, *Tectonics*, *22*, doi:10.1029/2002TC001397, in press, 2003.
- England, P., and G. Houseman, Role of lithospheric strength heterogeneities in the tectonics of Tibet and neighbouring regions, *Nature*, *315*, 297–301, 1985.
- England, P., and G. Houseman, Finite strain calculations of continental deformation: 2. Comparison with the India-Asia collision zone, *J. Geophys. Res.*, *91*(B3), 3664–3676, 1986.
- England, P. C., and G. A. Houseman, The mechanics of the Tibetan Plateau, *Philos. Trans. R. Soc. London*, *326*, 301–320, 1988.
- England, P., and P. Molnar, Right-lateral shear and rotation as the explanation for strike-slip faulting in eastern Tibet, *Nature*, *344*, 140–142, 1990.
- England, P., and P. Molnar, The field of crustal velocity in Asia calculated from Quaternary rates of slip on faults, *Geophys. J. Int.*, *130*, 551–582, 1997.
- England, P., G. Houseman, and L. Sonder, Length scales for continental deformation in convergent, divergent, and strike-slip environments: Analytical and approximate solutions for a thin viscous sheet model, *J. Geophys. Res.*, *90*(B5), 3551–3557, 1985.
- Fisher, R. A., Dispersion on a sphere, *Proc. R. Soc. London, Ser. A*, *217*, 295–305, 1953.
- Frost, G. M., R. S. Coe, Z. Meng, Z. Peng, Y. Chen, V. Courtillot, G. Peltzer, P. Tapponnier, and J. P. Avouac, Preliminary Early Cretaceous paleomagnetic results from the Gansu Corridor, China, *Earth Planet. Sci. Lett.*, *129*, 217–232, 1995.
- Gansu Bureau of Geology and Mineral Resources, *Regional Geology of Gansu Province* (in Chinese with English summary), 690 pp., Geol. Publ. House, Beijing, 1989.
- Geissman, J. W., B. C. Burchfiel, E. Wang, L. Chen, and J. Yin, Paleomagnetic data and Cenozoic tectonic rotations in northern Indochina, with implications for middle Cenozoic extrusion of crust south of the Ailao Shan shear zone, *Geol. Soc. Am. Abstr. Programs*, *33*, 43, 2001.
- George, A. D., S. J. Marshallsea, K.-H. Wyrwoll, J. Chen, and Y. Lu, Miocene cooling in the Northern Qilian Shan, northeastern margin of the Tibetan Plateau, revealed by apatite fission-track and vitrinite-reflectance analysis, *Geology*, *29*(10), 939–942, 2001.
- Halim, N., J. P. Cogné, Y. Chen, R. Atasiesi, J. Besse, V. Courtillot, S. Gilder, J. Marcoux, and R. L. Zhao, New Cretaceous and early Tertiary paleomagnetic results from Xining-Lanzhou basin, Kunlun and Qiangtang blocks, China: Implications on the geodynamic evolution of Asia., *J. Geophys. Res.*, *103*(B9), 21,025–21,045, 1998.
- Holt, W. E., and A. J. Haines, Velocity fields in deforming Asia from the inversion of earthquake-released strains, *Tectonics*, *12*(1), 1–20, 1993.
- Holt, W. E., M. Li, and A. J. Haines, Earthquake strain rates and instantaneous relative motion within central and east Asia, *Geophys. J. Int.*, *122*, 569–593, 1995.
- Holt, W. E., N. Chamot-Rooke, X. Le Pichon, A. J. Haines, B. Shen-Tu, and J. Ren, Velocity field in Asia inferred from Quaternary fault slip rates and Global Positioning System observations, *J. Geophys. Res.*, *105*(B8), 19,185–19,209, 2000.
- Huang, K., N. D. Opdyke, J. Li, and X. Peng, Paleomagnetism of Cretaceous rocks from eastern Qiangtang terrane of Tibet, *J. Geophys. Res.*, *97*(B2), 1789–1799, 1992.
- Jolivet, M., F. Roger, N. Arnaud, M. Brunel, P. Tapponnier, and D. Seward, Histoire de l'exhumation de l'Altyn Shan: indications sur l'âge de la subduction du bloc du Tarim sous le système de l'Altyn Tagh (Nord Tibet), *C. R. Acad. Sci., Ser. IIA*, *329*, 749–755, 1999.
- Jolivet, M., M. Brunel, D. Seward, Z. Xu, J. Yang, F. Roger, P. Tapponnier, J. Malavieille, N. Arnaud, and C. Wu, Mesozoic and Cenozoic tectonics of the northern edge of the Tibetan Plateau: Fission-track constraints, *Tectonophysics*, 2002.
- Kirschvink, J. L., The least-square line and plane and the analysis of paleomagnetic data, *Geophys. J. R. Astron. Soc.*, *62*, 699–718, 1980.
- Kong, X., and P. Bird, Neotectonics of Asia: thin-shell finite-element models with faults, in *Tectonic Evolution of Asia, Rubey Volume IX*, edited by A. Yin and T. M. Harrison, pp. 18–35, Cambridge Univ. Press, New York, 1996.
- Le Pichon, X., M. Fournier, and L. Jolivet, Kinematics, topography, shortening, and extrusion in the India-Eurasia collision, *Tectonics*, *11*(6), 1085–1098, 1992.
- Lin, J., and D. R. Watts, Paleomagnetic results from the Tibetan Plateau, *Philos. Trans. R. Soc. London*, *327*, 239–262, 1988.
- Ma, X., Z. Yang, and L. Xing, The Lower Cretaceous reference pole for the North China and its tectonic implications, *Geophys. J. Int.*, *115*, 323–331, 1993.
- McFadden, P. L., A new fold test for palaeomagnetic studies, *Geophys. J. Int.*, *103*, 163–169, 1990.

- McFadden, P. L., and M. W. McElhinny, Classification of the reversal test in palaeomagnetism, *Geophys. J. Int.*, 103, 725–729, 1990.
- Meng, Q.-R., J.-M. Hu, and F.-Z. Yang, Timing and magnitude of displacement on the Altyn Tagh fault: constraints from stratigraphic correlation of adjoining Tarim and Qaidam basins, NW China, *Terra Nova*, 13(2), 86–91, 2001.
- Mériaux, A., F. J. Ryerson, P. Tapponnier, J. Van der Woerd, R. C. Finkel, M. W. Caffee, C. Lasserre, X. Xu, H. Li, and Z. Xu, Fast extrusion of the Tibet Plateau: A 3 cm/yr, 100 kyr slip-rate on the Altyn Tagh Fault, *Eos Trans. AGU*, 81(48), Abstract T62D-07, 2000.
- Meyer, B., P. Tapponnier, L. Bourjot, F. Metivier, Y. Gaudemer, G. Peltzer, G. Shummin, and C. Zhitai, Crustal thickening in the Gansu-Qinghai, lithospheric mantle, oblique and strike-slip controlled growth of the Tibetan Plateau, *Geophys. J. Int.*, 135, 1–47, 1998.
- Molnar, P., and Q. Deng, Faulting associated with large earthquakes and the average rate of deformation in central and eastern Asia, *J. Geophys. Res.*, 89(B7), 6203–6227, 1984.
- Molnar, P., and H. Lyon-Caen, Fault plane solutions of earthquakes and active tectonics of the Tibetan Plateau and its margins, *Geophys. J. Int.*, 99, 123–153, 1989.
- Molnar, P., and P. Tapponnier, Cenozoic tectonics of Asia: effects of a continental collision, *Science*, 189(4201), 419–426, 1975.
- Molnar, P., B. C. Burchfiel, L. K'uangyi, and Z. Ziyun, Geomorphic evidence for active faulting in the Altyn Tagh and northern Tibet and qualitative estimates of its contribution to the convergence of India and Eurasia, *Geology*, 15(3), 249–253, 1987.
- Molnar, P., P. England, and J. Martinod, Mantle dynamics, uplift of the Tibetan Plateau, and the Indian monsoon, *Rev. Geophys.*, 31(4), 357–396, 1993.
- Nelson, M. R., and C. H. Jones, Paleomagnetism and crustal rotations along a shear zone, Las Vegas Range, southern Nevada, *Tectonics*, 6(1), 13–33, 1987.
- Otofujii, Y., S. Inoue, S. Funahara, F. Murata, and X. Zheng, Palaeomagnetic study of eastern Tibet—deformation of the Three Rivers region, *Geophys. J. Int.*, 103, 85–94, 1990.
- Peltzer, G., and F. Saucier, Present-day kinematics of Asia derived from geologic fault rates, *J. Geophys. Res.*, 101(B12), 27,943–27,956, 1996.
- Peltzer, G., and P. Tapponnier, Formation and evolution of strike-slip faults, rifts, and basins during the India-Asia collision: an experimental approach, *J. Geophys. Res.*, 93(B12), 15,085–15,117, 1988.
- Peltzer, G., P. Tapponnier, and R. Armijo, Magnitude of Late Quaternary, left-lateral movement along the north edge of Tibet, *Science*, 246, 1285–1289, 1989.
- Qinghai Bureau of Geology and Mineral Resources, *Regional Geology of the Qinghai Province*, 662 pp., Geol. Publ. House, Beijing, 1991.
- Ritts, B. D., and U. Biffi, Magnitude of post-Middle Jurassic (Bajocian) displacement on the central Altyn Tagh fault system, northwest China, *Geol. Soc. Am. Bull.*, 112, 61–74, 2000.
- Robinson, A. C., A. Yin, C. A. Menold, X. Chen, and W. X. Feng, Tertiary Shortening along the Eastern Portion of the North Qaidam Thrust System, *Eos Trans. AGU*, 83(47), Fall Meet. Suppl., Abstract T51B-1158, 2002a.
- Robinson, D. M., G. Dupont-Nivet, G. E. Gehrels, and Y. Zhang, The Tula uplift, northwestern China: Evidence for regional tectonism of the northern Tibetan Plateau, *Geol. Soc. Am. Bull.*, 115(1), 35–47, 2002b.
- Royden, L. H., B. C. Burchfiel, R. W. King, E. W. Wang, Z. Chen, F. Shen, and Y. Liu, Surface deformation and lower crustal flow in eastern Tibet, *Science*, 276, 788–790, 1997.
- Rumelhart, P. E., A. Yin, E. Cowgill, R. F. Butler, Q. Zhang, and X.-F. Wang, Cenozoic vertical-axis rotation of the Altyn Tagh fault system, *Geology*, 27(9), 819–822, 1999.
- Shen, Z. K., M. Wang, Y. Li, D. J. Jackson, A. Yin, D. Dong, and P. Fang, Crustal deformation along the Altyn Tagh Fault system, western China, from GPS, *J. Geophys. Res.*, 106(12), 30,607–30,621, 2001.
- Sobel, E. R., N. Arnaud, M. Jolivet, B. D. Ritts, and M. Brunel, Jurassic to Cenozoic exhumation history of the Altyn Tagh range, NW China, constrained by Ar/Ar and apatite fission track thermochronology, in *Paleozoic and Mesozoic Tectonic Evolution of Central and Eastern Asia: From Continental Assembly to Intracontinental Deformation*, edited by M. S. Hendrix and G. A. Davis, *Geol. Soc. Am. Mem.*, 194, 247–267, 2001.
- Sonder, L. J., and P. England, Vertical averages of rheology of the continental lithosphere: Relation to thin sheet parameters, *Earth Planet. Sci. Lett.*, 77, 81–90, 1986.
- Sonder, L. J., P. C. England, and G. A. Houseman, Continuum calculations of continental deformation in transcurrent environments, *J. Geophys. Res.*, 91(B5), 4797–4810, 1986.
- Sun, Z., Z. Yang, and T. Yang, Early Cretaceous paleomagnetic results from the Haiyuan area and its tectonic implications, *Acta Geophys. Sin.*, 44(5), 675–683, 2001.
- Tapponnier, P., G. Peltzer, A. Y. Le Dain, R. Armijo, and P. Cobbold, Propagating extrusion tectonics in Asia: new insights from simple experiments with plasticine, *Geology*, 10, 611–616, 1982.
- Tapponnier, P., G. Peltzer, and R. Armijo, On the mechanics of the collision between India and Asia, in *Collision Tectonics*, edited by M. P. Coward and A. C. Ries, pp. 115–158, Blackwell Sci., Malden, Mass., 1986.
- Tapponnier, P., Z. Xu, F. Roger, B. Meyer, N. Arnaud, G. Wittlinger, and J. Yang, Oblique stepwise rise and growth of the Tibetan Plateau, *Science*, 294, 1671–1677, 2001.
- Thomas, J.-C., H. Perroud, P. R. Cobbold, M. L. Bazhenov, V. S. Burtman, A. Chauvin, and I. S. Sadybakasov, A paleomagnetic study of Tertiary formations from the Kyrgyz Tien-Shan and its tectonic implications, *J. Geophys. Res.*, 98(B6), 9571–9589, 1993.
- Thomas, J.-C., A. Chauvin, D. Gapais, M. L. Bazhenov, H. Perroud, P. R. Cobbold, and V. S. Burtman, Paleomagnetic evidence for Cenozoic block rotations in the Tadjick depression (central Asia), *J. Geophys. Res.*, 99(B8), 15,141–15,160, 1994.
- van der Woerd, J., F. J. Ryerson, P. Tapponnier, Y. Gaudemer, R. Finkel, A. S. Mériaux, M. Caffee, Z. Guoguang, and H. Qunlu, Holocene left-slip rate determined by cosmogenic surface dating on the Xidatan segment of the Kunlun fault (Qinghai, China), *Geology*, 26(268), 695–698, 1998.
- Vincent, S. J., and M. B. Allen, Evolution of the Minle and Chaoshui Basins, China: Implication for Mesozoic strike-slip basin formation in Central Asia, *Geol. Soc. Am. Bull.*, 111(5), 725–742, 1999.
- Wang, Q., and M. P. Coward, The Chaidam basin (NW China): Formation and hydrocarbon potential, *J. Pet. Geol.*, 13(1), 93–112, 1990.
- Wang, Q. M., and M. P. Coward, The Jiuxi basin, Hexi corridor, NW China: Foreland structural features and hydrocarbon potential, *J. Pet. Geol.*, 16(2), 169–182, 1993.
- Washburn, Z., J. R. Arrowsmith, S. L. Forman, E. Cowgill, W. Xiaofeng, Y. Zhang, and Z. Chen, Late Holocene earthquake history of the central Altyn Tagh fault, China, *Geology*, 29(11), 1051–1054, 2001.
- Watson, G. S., and R. J. Enkin, The fold test in paleomagnetism as a parameter estimation problem, *Geophys. Res. Lett.*, 20(19), 2135–2137, 1993.
- Wittlinger, G., P. Tapponnier, G. Poupinet, J. Mei, S. Danian, G. Herquel, and F. Masson, Tomographic evidence for localized lithospheric shear along the Altyn Tagh fault, *Science*, 282, 74–76, 1998.
- Xinjiang Bureau of Geological and Mineral Resources (XBGRM), *Regional geology of the Xinjiang Uygur Autonomous Region*, 841 pp., Geol. Publ., Beijing, 1993.
- Yang, T., Z. Yang, Z. Sun, and A. Lin, New Early Cretaceous paleomagnetic results from Qilian orogenic belt and its tectonic implications, *Sci. China, Ser. D*, 45(6), 565–576, 2002.
- Yin, A., and M. T. Harrison, Geologic evolution of the Himalayan-Tibetan orogen, *Annu. Rev. Earth Planet. Sci.*, 28, 211–280, 2000.
- Yin, A., et al., Tectonic history of the Altyn Tagh fault system in northern Tibet inferred from Cenozoic sedimentation, *Geol. Soc. Am. Bull.*, 114(10), 1257–1295, 2002.
- Yue, Y., B. D. Ritts, and S. A. Graham, Initiation and long-term slip history of the Altyn Tagh fault, *Int. Geol. Rev.*, 43, 1087–1093, 2001.

R. F. Butler, Department of Geosciences, University of Arizona, Tucson, AZ 85721, USA. (butler@geo.arizona.edu)

X. Chen, Institute of Geomechanics, Beijing 10081, China. (xhchen0419@sina.com)

G. Dupont-Nivet, Faculty of Earth Sciences, Paleomagnetic Laboratory - "Fort Hoofdijk", Utrecht University, Budapestlaan 17, 3584 CD Utrecht, Netherlands. (gdn@geo.uu.nl)

A. Yin, Department of Earth and Space Sciences, University of California, Los Angeles, 595 Charles Young Drive East, 3806 Geology Building, Los Angeles, CA 90095-1567, USA. (yin@ess.ucla.edu)